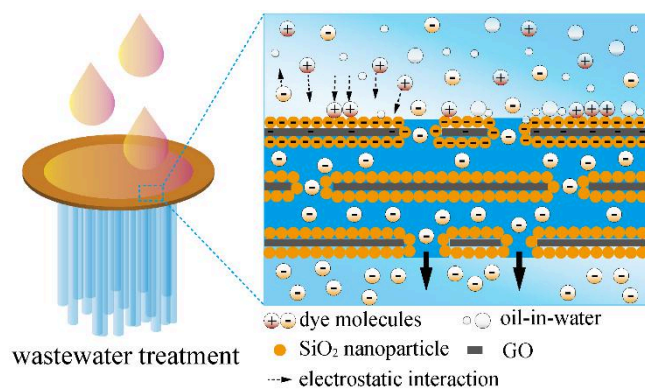


Well-structured 3D channels within GO-based membranes enable ultrafast wastewater treatment

Graphical Table of Contents



The well-structured 3D water channels within GO-based membranes can synchronize ultrahigh water permeance and purification performance for highly efficient wastewater treatment.

Well-structured 3D channels within GO-based membranes enable ultrafast wastewater treatment

Huaqiang Fu^{1,#}, Zhe Wang^{2,3,#}, Peng Li^{2,*}, Wei Qian², Zixin Zhang¹, Xin Zhao², Hao Feng¹, Zhugen Yang⁴, Zongkui Kou^{1,3,*}, and Daping He^{1,2,*}

¹ School of Materials Science and Engineering, Wuhan University of Technology, Wuhan 430070, China

² Hubei Engineering Research Center of RF-Microwave Technology and Application, School of Science, Wuhan University of Technology, Wuhan 430070, China

³ State Key Laboratory of Advanced Technology for Materials Synthesis and Processing, Wuhan University of Technology, Wuhan 430070, China

⁴ School of Water, Energy and Environment, Cranfield University, Cranfield MK43 0AL, UK

These authors contributed equally.

* Corresponding Author.

Email-address: lipeng871120@whut.edu.cn (Peng Li), zongkuikou@whut.edu.cn (Zongkui Kou), hedaping@whut.edu.cn (Daping He).

Abstract

Graphene oxide (GO)-based membranes have been widely studied for realizing efficient wastewater treatment, due to their easily functionalizable surfaces and tunable interlayer structures. However, the irregular structure of water channels within GO-based membrane has largely confined water permeance and prevented the simultaneous improvement of purification performance. Herein, we purposely construct the well-structured 3D water channels featuring regular and negatively-charged properties in the GO/SiO₂ composite membrane via in situ close-packing assembly of SiO₂ nanoparticles onto GO nanosheets. Such regular 3D channels can improve the water permeance to a record-high value of $33431.5 \pm 559.9 \text{ L m}^{-2} \text{ h}^{-1} (\text{LMH}) \text{ bar}^{-1}$, which is several-fold higher than those of current state-of-the-art GO-based membranes. We further demonstrate that benefiting from negative charges on both GO and SiO₂, these negatively-charged 3D channels enable the charge selectivity well toward dye in wastewater where the rejection for positive-charged and negative-charged dye molecules is 99.6% vs. 7.2%, respectively. The 3D channels can also accelerate oil/water (O/W) separation process, in which the O/W permeance and oil rejection can reach $19589.2 \pm 1189.7 \text{ LMH bar}^{-1}$ and 98.2%, respectively. The present work unveils the positive role of well-structured 3D channels on synchronizing the remarkable improvement of both water permeance and purification performance for highly efficient wastewater treatment.

Keywords: graphene oxide, membranes, wastewater treatment, water channels, charge-selectivity

1 Introduction

The ever-growing global water scarcity and effluent discharge have made efficient and economic wastewater treatment an urgent task [1,2]. The expected demands of wastewater (*e.g.* organic dye solutions and oil emulsions) for pollution-free emission or recycling utilization, have necessitated purification treatments that achieve pollutant elimination or retention of reusable solutes [3–5]. Many wastewater treatment processes have been developed, among which pressure driven membrane-based purification technology has attracted enormous attention due to its simplicity and low environmental impact [6]. However, both the inadequate water permeance and purification performance are hindering large scale application of existing membranes [7,8].

Graphene oxide (GO)-based membranes with functionalizable surfaces, and adjustable interlayer structures have been demonstrated with great potential to realize high water permeance and good purification performance, thus capturing lots of interest in recent years [9,10]. Specially, the water permeance of GO-based membranes was significantly enhanced by optimizing interlaminar water channels [11]. For example, water channels was improved by introducing zero-dimension carbon dots inside GO membranes, several-fold increasing the water permeance from $53 \text{ L m}^{-2} \text{ h}^{-1} (\text{LMH}) \text{ bar}^{-1}$ to 439 LMH bar^{-1} [12]. Water channels of one-dimension established with nanotubes at interlayers of GO membranes can enhance the water permeance to about 700 LMH bar^{-1} [13,14]. Furthermore, the water permeance of GO membranes with interlaminar two-dimensional water channels can be dramatically

promoted to 4536 LMH bar⁻¹ [15]. Unfortunately, the generation rate of wastewater in one ordinary factory is still far beyond the processing efficiency provided by current GO-based membranes [16,17]. The improvement bottleneck of water permeance in the GO-based membrane mainly derives from irregular water channels inside, which are randomly distributed and produced around three-dimensional (3D) voids of GO matrix [18]. Such irregular water channels can result in vast reservation of pristine confinements of GO interlayers [19,20], where plugging can take place during water transport due to strong capillary force and the narrow nanochannels [13]. The well-structured 3D water channels are therefore highly desired to elevate the water permeance to a largest level, but their construction within GO membranes remains a crucial challenging.

Although promising in improving water permeability by constructing 3D water channels [21,22], how to tradeoff the high water permeance and purification performance is another challenge [23,24]. Theoretically, the purification mechanisms of the GO membrane include physical size sieving and electrostatic adsorbing toward specific solutes [25,26]. The sieving is accomplished by microporous defects derived from imperfect stacking [27], and interlaminar confinement of GO nanosheets [28]. The 3D water channels will inevitably expand the pore diameters, resulting in a serious degradation on the purification capacity of GO membranes [29,30]. Therefore, improving water permeance without sacrificing purification performance has become nearly impossible in conventionally designed membranes with 3D water channels.

In this work, we report the construction of regular and negatively-charged 3D

water channels within GO membranes by *in situ* and close-packing growing of SiO₂ nanoparticles onto stacked GO nanosheets for synchronizing ultrahigh water permeance and purification performance. The water permeance of membrane with such well-structured 3D water channels can reach 33431.5±559.9 LMH bar⁻¹, which is a record-high value compared with the state-of-the-art membranes. Simultaneously, the negatively-charged 3D water channels are demonstrated to promote the charge selectivity of membranes toward dye molecules, in which the optimum rejections for positive-charged and negative-charged dye molecules are 99.6% and 7.2%, respectively. Besides, the 3D water channels can facilitate the oil/water (O/W) separation process, in which the O/W permeance and oil rejection can be boosted to 19589.2±1189.7 LMH bar⁻¹ and 98.2%, respectively.

2 Results and discussion

The regular and negatively-charged 3D water channels are constructed by assembling close-packing SiO₂ nanoparticles on stacked GO nanosheets, based on *in situ* hydrolysis strategy of tetraethyl orthosilicate (TEOS) (Fig. 1(a)) [31,32]. Such well-structured SiO₂ nanoparticles can expand the micropores, and broaden the interlayer spacing to improve water permeability of the GO membrane. Moreover, the hydrophilic close-packing SiO₂ nanoparticles can facilitate water transport [33,34]. Thus, we speculate that they can serve as 3D water channels. In contrast, water can hardly penetrate through pure GO membranes with tiny microporous and narrow interlayer spacing [35,36], as depicted in Fig. 1(b), illustrating the crucial role of 3D water channels.

To obtain close-packing structure of SiO₂ nanoparticles on GO nanosheets, the growth behaviors were firstly investigated. We denote the dispersions and the as-prepared membranes as GO/SiO₂-x, where x (0, 0.1, 0.3, 0.5, 1.0, 2.0 and 3.0) represents the additive volume (mL) of TEOS. By tuning the value of x, the growth behavior of SiO₂ nanoparticles displays as two stages: irregular distribution and close-packing (Fig. 2(a)). TEM images of GO/SiO₂ dispersions confirm that the particle size (PS) and coverage rate (CR) of SiO₂ nanoparticles vary when altering the value of x (Fig. S1 in the Electronic Supplementary Material (ESM)). For x=0, the pristine GO surface without any nanoparticles is set as the comparison template (Fig. 2(b)). Irregular distribution stage occurs when x values at below 0.5, featured by CR of SiO₂ nanoparticles beneath 100%, and slightly fluctuated PS (Fig. 2(c) and 2(d)). Notably, with x value exceeding 0.5, the CR reaches 100%, verifying the close-packing stage (Fig. 2(e)-(g)). Further, the average PS dramatically increases from 15.44 nm to 60.86 nm, implying the controllable and optimizable structure in close-packing stage.

The abundant functional groups on GO nanosheets are confirmed by the intense O 1s peak in the X-ray photoelectron spectroscopy spectra of GO membranes (Fig. S2 in the ESM), and the equally distributed elemental mapping of O on the GO membrane surface (Fig. S3 in the ESM), which serve as the nucleation sites for *in situ* growth of SiO₂ nanoparticles [31,32]. With the addition of TEOS dosage, the nucleation sites are gradually occupied by SiO₂ nanoparticles until completely filled to form close-packing structure (Fig. 2(b)-(g) and Fig. S4 in the ESM). At the

close-packing stage, these SiO₂ nanoparticles grows up rapidly due to lack of extra nucleation sites, conforming to the growth kinetics of colloid in sol-gel method [33].

GO/SiO₂-x membranes are fabricated on the mixed cellulose (MCE) substrates in vacuum-assisted self-assembly method, by using 0.5 mL GO/SiO₂-x dispersions (Fig. S5 in the ESM). Apparently, the *in situ* grown SiO₂ nanoparticles cannot deteriorate the membrane-forming ability (Fig. 3(a) and 3(b)), mainly resulted from the cross-linking of functional groups under hydrogen bond [34,37]. When without SiO₂ nanoparticles, the pure GO membrane presents a dense and continuous surface (Fig. 3(c)). On the contrary, the surface becomes cracked gradually with the increasing contents of SiO₂ nanoparticles, especially at the close-packing process (Fig. S6 in the ESM). The fluffiest and most porous surface was obtained in the GO/SiO₂-2.0 membrane (Fig. 3(d)). In the cross-sectional SEM image, GO/SiO₂-x membranes prepared by using 0.5 mL dispersions exhibits unquantifiable thickness and indistinguishable structure (Fig. S7 in the ESM). We thus increased the addition of GO/SiO₂-x dispersions to assemble thicker membranes. As depicted in Fig. 3(e), the pure GO membrane acquires the most compact stacking layers, producing narrow interlaminar water pathways. While the stacked structure of GO/SiO₂-2.0 membrane becomes remarkably fluffy (Fig. 3(f)), confirming the broadening of interlayer spacing. Moreover, the evenly distributed Si element certifies the interlinked SiO₂ nanoparticles on GO matrix (Fig. 3(g) and Fig. S8 in the ESM), which is consistent to our proposed scheme. The X-ray diffraction (XRD) patterns of GO/SiO₂-x membranes verify the crucial role of close-packing SiO₂ nanoparticles in constructing

3D water channels (Fig. 3(h)). The interlayer spacing is calculated to have a positive correlation with the addition volume of TEOS, and widens from 0.752 nm to 0.782 nm which is identified as the regular distribution stage ($x < 0.5$). The characteristic peak disappears at the close-packing stage ($x \geq 0.5$), which indicates complete elimination of periodic stacked lattice of GO nanosheets, affirming the construction of interlinked 3D water channels at this stage.

The average pore widths of GO/SiO₂-0.5, 1.0 and 2.0 membranes are 4.89 nm, 11.86 nm and 13.40 nm, respectively (Fig. 3(i) and Fig. S9 in the ESM), verifying the controllable structure of 3D water channels by tuning the TEOS addition. Depending on TEOS dosage, the composite membrane also illustrates adjustable hydrophilicity as shown in Fig. 3(j). The variance of contact angle on membrane also matches well with the structure evolution of SiO₂ nanoparticles within membrane. At the irregular distribution stage ($x < 0.5$), the increase of contact angles mainly originates from reduction in the exposure level of hydrophilic functional groups. For the close-packing stage ($x \geq 0.5$), the contact angle declines dramatically, confirming predominant correlation between structure of 3D water channels and hydrophilicity of membranes, supporting the crucial role of 3D water channels. We infer that the increased pore width of 3D water channels can afford improved capillary action to optimize hydrophilicity. Notably, the GO/SiO₂-2.0 membrane exhibits super hydrophilicity (Movie S1), in which the contact angle plunges from 15.4 ° to less than 3 ° within 1 second, which is conducive to high water permeability [38].

To explore the positive effect of 3D water channels on water permeable

performance, water flux test was carried out under -0.08 MPa (Fig. 4(a)). As water channels are irregularly distributed ($x < 0.5$), the water permeance slightly increases beneath the order of 10^3 LMH bar⁻¹. With regular 3D water channels, the water permeance increases dramatically to 33431.5 ± 559.9 LMH bar⁻¹ in the GO/SiO₂-2.0 membrane (the extremely rapid water penetrant process can be seen in Movie S2), which is approximately three orders of magnitude improvement compared to pure GO membrane (40.6 LMH bar⁻¹). With further increasing x value to 3.0, the water permeance slightly declines to 32464.2 LMH bar⁻¹, probably resulted from saturated growth of SiO₂ nanoparticles on GO nanosheets.

The GO/SiO₂-2.0 membrane with optimal 3D water channels was used for permeance stability test (Fig. 4(b)). During continuous filtering operation for 400 minutes, the water permeance stabilizes at an average of 33332.7 LMH bar⁻¹, of which the variance is only 337.3. The outstanding stability of water permeance is originated from solid 3D water channels in the GO/SiO₂-2.0 membrane [39,40]. As confirmed by zeta potential measurement (inset in Fig. 4(b)), the negative potentials SiO₂ nanoparticles helps maintain the mesoporous structure of 3D water channels under pressure. Meanwhile the SiO₂ nanoparticles with multiple functional groups can crosslink with each other [31,32], and immobilize on GO nanosheets [33,34] for robust construction of 3D water channels. With increasing filtering pressure, the stable water permeance and linearly augmented water flux confirms the solid structure of 3D water channels (Fig. 4(c)). Moreover, the fitting goodness between water permeance and membrane thickness reaches 0.995 (Fig. 4(d) and Fig. S10 in the

ESM), also demonstrating the superiority and structure stability of regular 3D water channels.

For comparison, water permeance stability test of GO+SiO₂-2.0 membranes prepared by mechanical mixing of GO nanosheets and SiO₂-2.0 colloids was carried out (Fig. S11 in the ESM). To exclude the size effect, the close size and same content of SiO₂ nanoparticles in the preparation of both GO+SiO₂-2.0 and GO/SiO₂-2.0 membranes are applied (Fig. S12 in the ESM). The GO+SiO₂-2.0 membrane acquires a maximum water permeance of 4269.5 LMH bar⁻¹ (Fig. S13 in the ESM), which reaches the peak value of reported membranes prepared by mechanical mixing of GO and SiO₂ nanoparticles, confirming the data reliability in our work [41,42]. But the permeance value promptly descends to 1946.7 LMH bar⁻¹ within 10 minutes. The characteristic XRD peak of GO demonstrates still existed GO interlayer spacing within GO+SiO₂-2.0 membrane (Fig. S14 in the ESM), leading to relatively low water permeance compared with GO/SiO₂-2.0 membranes (Fig. S15 in the ESM). Moreover, TEM images confirms the irregular distributed water channels within GO+SiO₂-2.0 membranes (Fig. S16 in the ESM), reflecting the crucial role of 3D water channels in improving membrane reliability.

Purification performance is another key index for membrane evaluation. In this work, we use three kinds of common industrial dye solutions to test [43], including methylene blue (MB), butyl rhodamine B (BRB) and methyl orange (MO). The membrane with 3D water channels can sustain significant charge-selectivity toward dye molecules (Fig. 5(a)). Specially, the rejections of GO/SiO₂-2.0 membranes toward

positive-charged and negative-charged dye molecules are 99.6% and 7.2%, respectively. Besides, the GO/SiO₂-2.0 membrane with optimum 3D water channels exhibit unchanged MB rejections when dye volume is below 100 ml, verifying its reliability (Fig. 5(b)). Due to ultrahigh water permeability and excellent charge-selectivity toward dye molecules, the GO/SiO₂-2.0 membrane with optimal 3D water channels can be applied to highly efficient wastewater treatment, such as elimination of pollutants (Fig. 5(c) and 5(d)) or selective reservation of reusable solutes (Fig. 5(e) and 5(f)). In addition, the GO/SiO₂-2.0 membrane also displays excellent O/W separation performance. As shown in Fig. 5(g), diesel and soybean oil were prepared as oil emulsions to simulate emulsified oil in industrial wastewater. By using GO/SiO₂-2.0 membranes, the O/W permeance achieves 19589.2±1189.7 LMH bar⁻¹, and the rejections of diesel and soybean oil emulsions exceed 99.0% and 98.2%, respectively (Fig. 5(h)).

Compared with representative GO-based membranes in the literature (Table S1 in the ESM), the GO/SiO₂-2.0 membrane with optimal 3D water channels exhibits a historically high water permeance, which is several-fold higher than the reported value (Fig. 5(i)). Synchronously, the optimal membrane reported in this work can maintain outstanding purification performance, validating the strategy feasibility and practicability of constructing 3D water channels within GO membranes.

The pore diameters of GO/SiO₂-2.0 membranes mainly distribute at the range between 30 nm to 100 nm (Fig. S9 in the ESM), which is extremely larger than the size of dye molecules [43]. Owing to expansion of the pore width, the MO rejection

of GO/SiO₂-2.0 membranes deduces by half compared to pure GO membrane (Fig. 5(a)). Therefore, synchronizing high water permeance and excellent purification performance by constructing of 3D water channels in GO-based membranes are counterintuitive. The retention of excellent purification performance mainly results from enhanced negative surface potential by 3D water channels (inset in Fig. 4(b)). As shown in Fig. 6, the enhanced negative surface potential can promote electrostatic adsorption toward positive-charged dye molecules, and repulsion to negative-charged dye molecules, respectively [44,45]. Thus, the GO/SiO₂-2.0 membrane exhibits excellent dye separation performance under ultrahigh water flux. Moreover, the MB rejection of the GO/SiO₂-2.0 membrane plunges fastly when MB volume exceeds 100 ml (Fig. 5(b)), mainly resulted from electrostatic saturation [41], further confirming that the dye removal mechanism are based on electrostatic reaction. In addition, benefiting from oil adsorbing of porous structure [46] and underwater oleophobic interface of SiO₂ nanoparticles [41,47], the 3D water channels therefore improve the O/W separation efficiency.

3 Conclusions

In conclusion, we have successfully addressed the challenge that achieving synchronous ultrahigh water permeance and purification performance in GO-based membranes, by constructing regular and negatively-charged 3D water channels through close-packing assembling of SiO₂ nanoparticles onto stacked GO nanosheets. The water permeance reaches a record-high value of 33431.5±559.9 LMH bar⁻¹, which is several-fold exceeding that of reported GO-based membranes. The ultrahigh

water permeance can be maintained during continuous filtering operation for over 400 minutes, demonstrating the structural stability of such 3D water channels. Synchronously, the membrane with optimal 3D water channels can maintain outstanding charge selectivity toward dye molecules, in which the rejection of positive-charged and negative-charged dye molecules can achieve 99.6% and 7.2%, respectively. In addition, the 3D water channels can improve oil/water (O/W) separation efficiency, in which the O/W permeance and oil rejection can reach 19589.2 ± 1189.7 LMH bar⁻¹ and 98.2%. These results validate the strategy feasibility of constructed regular and charged 3D water channels within GO membranes, offering great potential in the fields of highly efficient wastewater treatment.

Methods

Materials. GO (4.5 wt.%) was purchased from Wuhan Hanene Technology Co., Ltd. MCE substrates (diameter: 50 mm, pore size: 0.45 μ m) were bought from Haining Guodian Taoyuan Medical Chemical Instrument Factory. TEOS and ammonium hydroxide (NH₃ · H₂O) solution were obtained from Shanghai Macklin Biochemical Co., Ltd. All the other chemicals (alcohol, dyes, Sodium dodecyl sulfate (SDS), *et al.*) used in this study were all purchased from Aladdin Industrial Co., Ltd.

Construction process of water channels in GO membranes. The construction of water channels was operated as follows. Firstly, deionized (DI) water and alcohol were mixed at the ratio of 1:19. Secondly, GO nanosheets was added into mixtures at a mass ratio of 2 mg/mL, and the obtained dispersions were mixed and degassed in the mixing homogenizer of SK-300S11 (Shashin Kagaku Co., ltd). Thirdly, TEOS

solution of x mL ($x=0, 0.1, 0.3, 0.5, 1.0, 2.0, 3.0$) was added into GO dispersions (50 mL) after adjusting the pH value to about 10 by $\text{NH}_3 \cdot \text{H}_2\text{O}$. Then, the GO/TEOS-x dispersions were ultrasonically treated for 3h (at this stage SiO_2 nanoparticles *in situ* grew up on GO surface) to get GO/ SiO_2 -x dispersions. Finally, the GO/ SiO_2 -x membranes (Fig. S5 in the ESM) were obtained through vacuum-assisted self-assembly using 0.5 mL GO/ SiO_2 -x dispersions and 10 mL DI water.

The GO+ SiO_2 -2.0 membrane was prepared based on mechanical mixing strategy. At first, SiO_2 -2.0 colloid was prepared by ultrasonically hydrolyzing of 2.0 mL TEOS in mixture of 45 mL DI water and 5 mL alcohol for 3 h, of which the pH was adjusted to 10 by $\text{NH}_3 \cdot \text{H}_2\text{O}$. Then GO was added into SiO_2 -2.0 colloid at a mass ratio of 2 mg/mL by ultrasonic mixing for 3 h to obtain GO+ SiO_2 -2.0 dispersions. Finally GO+ SiO_2 -2.0 membranes were prepared by vacuum-assisted self-assembly process using 0.5 mL GO+ SiO_2 -2.0 dispersion and 10 mL DI water. The prepared process can guarantee same contents of GO and SiO_2 particles in both GO+ SiO_2 -2.0 membrane and GO/ SiO_2 -2.0 membrane.

Characterization. Morphology and microstructure of GO/ SiO_2 -x membranes were characterized in scanning electron microscope (SEM, JSM-7610F Plus), transmission electron microscope (TEM, JEM-1400 Plus) and X-ray diffraction (XRD, Rigaku Smartlab, Cu $K\alpha$). Element mapping was conducted using Energy Dispersive Spectroscopy (EDS). Surface area and pore width of membranes were measured by Brunauer-Emmett-Teller (BET) surface area method using analyzing nitrogen sorption in a tristar-3020 instrument. Wet angle of water droplets on different

membranes were measured in the automatic contact angle measuring instrument (OCA35). Ultraviolet/visible (UV) spectrophotometer (Shimadzu UV-1800) was utilized to collect UV spectra of different filtrates before and after filtering.

Concentration measurement of dye solutions and O/W emulsions. The dyes (MB, BRB and MO) were all prepared with the concentration of 10 ppm, and O/W emulsions were prepared at the volume fraction of 0.5 % by ultrasonically mixing SDS (0.1 g), oil (2.5 mL, diesel and soybean oil) and DI water (497.5 mL) for 6 h. Due to samples of dyes solutions or O/W emulsions with different concentrations show positive correlation to spectral intensity of UV absorption at their characteristic wavelength, the concentration of samples can be detected using UV spectrophotometer [38,48]. As displayed in Fig. S17 and S18 in the ESM, the concentration and UV absorption intensity exhibit a good linear relationship with R -squared (R^2) value over 0.999. Hence, the concentration of dyes and oils can be determined according to the UV absorption intensity at their characteristic wavelengths.

Measurements of wastewater treatment performance. The water permeance, dye rejection and oil removal performance were carried out on a home-made dead-end vacuum filtration device with the effective area of 12.56 cm² at room temperature. At first, all the membranes are rinsed by DI water for 3 minutes at -0.08 MPa to obtain stable flux value, then the water permeance (J) is calculated as shown in equation (1). During measuring, all the collected data are averages of three samples during parallel tests.

$$J = \frac{\Delta V}{S \cdot T \cdot P} \quad (1)$$

Where ΔV (L) is the volume of penetrant water, S (m²) is the effective area of membranes, T (h) is the penetrant time, and P (bar) is the operating pressure.

Purification capacity is evaluated by rejection ratios of various dyes and O/W emulsions. The rejection ratios (R) can be computed according to equation (2).

$$R = \left(1 - \frac{C_b}{C_a}\right) \times 100\% \quad (2)$$

Where C_b is the original concentration of filtrates before filtering, and C_a represents the concentration of filtrates after filtering.

Acknowledgements

The authors acknowledge financial support from UK NERC Fellowship (NE/R013349/2).

Electronic Supplementary Material: Supplementary material (Photographs, TEM images of SiO₂ nanoparticles of GO/SiO₂-x dispersions, GO+SiO₂-2.0 dispersions and SiO₂-2.0 colloids; Surface SEM images, cross-sectional SEM images, elemental mapping images and Brunauer-Emmett-Teller surface measurement results of GO/SiO₂-x membranes; Water permeance, XRD patterns of GO+SiO₂-2.0 and GO/SiO₂-2.0 membranes. UV spectrum of dye solutions and corresponding concentration-absorbance function analysis, UV spectrum of oil emulsions and corresponding volume fraction-absorbance function analysis; Performance comparisons of GO-based membranes in literatures; Videos of wetting process of DI water on GO/SiO₂-2.0 membranes; Videos of filtering process of GO/SiO₂-2.0 membranes under -0.08 MPa.) is available in the online version of this article at

http://dx.doi.org/10.1007/s12274-***-****- (automatically inserted by the publisher).

References

- [1] Mekonnen, M. M.; Hoekstra, A. Y. Four Billion People Facing Severe Water Scarcity. *Sci. Adv.* **2016**, *2* (2), e1500323.
- [2] Butler, E.; Hung, Y. T.; Ahmad, M. Al; Fu, Y. P. Treatment and Management of Industrial Dye Wastewater for Water Resources Protection. In *Natural Resources and Control Processes*; Springer International Publishing: Cham, 2016; pp 187–232.
- [3] Grant, S. B.; Saphores, J. D.; Feldman, D. L.; Hamilton, A. J.; Fletcher, T. D.; Cook, P. L. M.; Stewardson, M.; Sanders, B. F.; Levin, L. A.; Ambrose, R. F.; Deletic, A.; Brown, R.; Jiang, S. C.; Rosso, D.; Cooper, W. J.; Marusic, I. Taking the “Waste” Out of “Wastewater” for Human Water Security and Ecosystem Sustainability. *Science* **2012**, *337* (6095), 681–686.
- [4] Jassby, D.; Cath, T. Y.; Buisson, H. The Role of Nanotechnology in Industrial Water Treatment. *Nat. Nanotechnol.* **2018**, *13* (8), 670–672.
- [5] Alvarez, P. J. J.; Chan, C. K.; Elimelech, M.; Halas, N. J.; Villagrán, D. Emerging Opportunities for Nanotechnology to Enhance Water Security. *Nat. Nanotechnol.* **2018**, *13* (8), 634–641.
- [6] Obotey Ezugbe, E.; Rathilal, S. Membrane Technologies in Wastewater Treatment: A Review. *Membranes* **2020**, *10* (5), 89.
- [7] Shi, Z.; Zhang, W.; Zhang, F.; Liu, X.; Wang, D.; Jin, J.; Jiang, L. Ultrafast

- Separation of Emulsified Oil/Water Mixtures by Ultrathin Free-Standing Single-Walled Carbon Nanotube Network Films. *Adv. Mater.* **2013**, *25* (17), 2422–2427.
- [8] Idris, S. N. A.; Jullok, N. Evaluation of Commercial Reverse Osmosis and Forward Osmosis Membranes at Different Draw Solution Concentration in Pressure Retarded Osmosis Process. *Mater. Today Proc.* **2021**, *46*, 2065–2069.
- [9] Huang, H.; Ying, Y.; Peng, X. Graphene Oxide Nanosheet: An Emerging Star Material for Novel Separation Membranes. *J. Mater. Chem. A* **2014**, *2* (34), 13772–13782.
- [10] Sun, M.; Li, J. Graphene Oxide Membranes: Functional Structures, Preparation and Environmental Applications. *Nano Today* **2018**, *20*, 121–137.
- [11] Shen, J.; Liu, G.; Han, Y.; Jin, W. Artificial Channels for Confined Mass Transport at the Sub-Nanometre Scale. *Nat. Rev. Mater.* **2021**, *6* (4), 294–312.
- [12] Wang, W.; Eftekhari, E.; Zhu, G.; Zhang, X.; Yan, Z.; Li, Q. Graphene Oxide Membranes with Tunable Permeability Due to Embedded Carbon Dots. *Chem. Commun.* **2014**, *50* (86), 13089–13092.
- [13] Huang, H.; Song, Z.; Wei, N.; Shi, L.; Mao, Y.; Ying, Y.; Sun, L.; Xu, Z.; Peng, X. Ultrafast Viscous Water Flow through Nanostrand-Channelled Graphene Oxide Membranes. *Nat. Commun.* **2013**, *4* (1), 1-9.
- [14] Gao, S. J.; Qin, H.; Liu, P.; Jin, J. SWCNT-Intercalated GO Ultrathin Films for Ultrafast Separation of Molecules. *J. Mater. Chem. A* **2015**, *3* (12), 6649–6654.
- [15] Liu, Y.; Su, Y.; Guan, J.; Cao, J.; Zhang, R.; He, M.; Gao, K.; Zhou, L.; Jiang, Z.

- 2D Heterostructure Membranes with Sunlight-Driven Self-Cleaning Ability for Highly Efficient Oil–Water Separation. *Adv. Funct. Mater.* **2018**, 28 (13), 1–10. <https://doi.org/10.1002/adfm.201706545>.
- [16] Bhol, P.; Yadav, S.; Altaee, A.; Saxena, M.; Misra, P. K.; Samal, A. K. Graphene-Based Membranes for Water and Wastewater Treatment: A Review. *ACS Appl. Nano Mater.* **2021**, 4 (4), 3274–3293.
- [17] Keskin, B.; Ersahin, M. E.; Ozgun, H.; Koyuncu, I. Pilot and Full-Scale Applications of Membrane Processes for Textile Wastewater Treatment: A Critical Review. *J. Water Process Eng.* **2021**, 42, 102172.
- [18] Zhang, W.; Xu, H.; Xie, F.; Ma, X.; Niu, B.; Chen, M.; Zhang, H.; Zhang, Y.; Long, D. General Synthesis of Ultrafine Metal Oxide/Reduced Graphene Oxide Nanocomposites for Ultrahigh-Flux Nanofiltration Membrane. *Nat. Commun.* **2022**, 13 (1), 1–10.
- [19] Gao, S. J.; Qin, H.; Liu, P.; Jin, J. SWCNT-Intercalated GO Ultrathin Films for Ultrafast Separation of Molecules. *J. Mater. Chem. A* **2015**, 3 (12), 6649–6654.
- [20] Deng, H.; Zheng, Q.; Chen, H.; Huang, J.; Yan, H.; Ma, M.; Xia, M.; Pei, K.; Ni, H.; Ye, P. Graphene Oxide/Silica Composite Nanofiltration Membrane: Adjustment of the Channel of Water Permeation. *Sep. Purif. Technol.* **2022**, 278, 119440.
- [21] Feng, X.; Imran, Q.; Zhang, Y.; Sixdenier, L.; Lu, X.; Kaufman, G.; Gabinet, U.; Kawabata, K.; Elimelech, M.; Osuji, C. O. Precise Nanofiltration in a Fouling-Resistant Self-Assembled Membrane with Water-Continuous Transport

- Pathways. *Sci. Adv.* **2019**, *5* (8), 1–12.
- [22] Yousefi, N.; Lu, X.; Elimelech, M.; Tufenkji, N. Environmental Performance of Graphene-Based 3D Macrostructures. *Nat. Nanotechnol.* **2019**, *14* (2), 107–119.
- [23] Xu, Z.; Li, X.; Teng, K.; Zhou, B.; Ma, M.; Shan, M.; Jiao, K.; Qian, X.; Fan, J. High Flux and Rejection of Hierarchical Composite Membranes Based on Carbon Nanotube Network and Ultrathin Electrospun Nanofibrous Layer for Dye Removal. *J. Memb. Sci.* **2017**, *535*, 94–102.
- [24] Park, H. B.; Kamcev, J.; Robeson, L. M.; Elimelech, M.; Freeman, B. D. Maximizing the Right Stuff: The Trade-off between Membrane Permeability and Selectivity. *Science* **2017**, *356* (6343), eaab0530.
- [25] Liu, G.; Ye, H.; Li, A.; Zhu, C.; Jiang, H.; Liu, Y.; Han, K.; Zhou, Y. Graphene Oxide for High-Efficiency Separation Membranes: Role of Electrostatic Interactions. *Carbon* **2016**, *110*, 56–61.
- [26] Hong, S.; Constans, C.; Surmani Martins, M. V.; Seow, Y. C.; Guevara Carrió, J. A.; Garaj, S. Scalable Graphene-Based Membranes for Ionic Sieving with Ultrahigh Charge Selectivity. *Nano Lett.* **2017**, *17* (2), 728–732
- [27] Seo, D. H.; Pineda, S.; Woo, Y. C.; Xie, M.; Murdock, A. T.; Ang, E. Y. M.; Jiao, Y.; Park, M. J.; Lim, S. Il; Lawn, M.; Borghi, F. F.; Han, Z. J.; Gray, S.; Millar, G.; Du, A.; Shon, H. K.; Ng, T. Y.; Ostrikov, K. Anti-Fouling Graphene-Based Membranes for Effective Water Desalination. *Nat. Commun.* **2018**, *9* (1), 1–12.
- [28] Boukhvalov, D. W.; Katsnelson, M. I.; Son, Y. W. Origin of Anomalous Water Permeation through Graphene Oxide Membrane. *Nano Lett.* **2013**, *13* (8),

3930–3935.

- [29]Aba, N. F. D.; Chong, J. Y.; Wang, B.; Mattevi, C.; Li, K. Graphene Oxide Membranes on Ceramic Hollow Fibers – Microstructural Stability and Nanofiltration Performance. *J. Memb. Sci.* **2015**, *484*, 87–94.
- [30]Lai, G. S.; Lau, W. J.; Goh, P. S.; Ismail, A. F.; Yusof, N.; Tan, Y. H. Graphene Oxide Incorporated Thin Film Nanocomposite Nanofiltration Membrane for Enhanced Salt Removal Performance. *Desalination* **2016**, *387*, 14–24.
- [31]Li, J.; Cui, J.; Yang, J.; Ma, Y.; Qiu, H.; Yang, J. Silanized Graphene Oxide Reinforced Organofunctional Silane Composite Coatings for Corrosion Protection. *Prog. Org. Coatings* **2016**, *99*, 443–451.
- [32]Chen, S. L.; Dong, P.; Yang, G. H.; Yang, J. J. Kinetics of Formation of Monodisperse Colloidal Silica Particles through the Hydrolysis and Condensation of Tetraethylorthosilicate. *Ind. Eng. Chem. Res.* **1996**, *35* (12), 4487–4493.
- [33]Zhou, X.; Shi, T. One-Pot Hydrothermal Synthesis of a Mesoporous SiO₂–Graphene Hybrid with Tunable Surface Area and Pore Size. *Appl. Surf. Sci.* **2012**, *259*, 566–573.
- [34]Kou, L.; Gao, C. Making Silica Nanoparticle-Covered Graphene Oxide Nanohybrids as General Building Blocks for Large-Area Superhydrophilic Coatings. *Nanoscale* **2011**, *3* (2), 519–528.
- [35]Xu, W. L.; Fang, C.; Zhou, F.; Song, Z.; Liu, Q.; Qiao, R.; Yu, M. Self-Assembly: A Facile Way of Forming Ultrathin, High-Performance Graphene Oxide Membranes for Water Purification. *Nano Lett.* **2017**, *17* (5), 2928–2933.

- [36] Yang, Q.; Su, Y.; Chi, C.; Cherian, C. T.; Huang, K.; Kravets, V. G.; Wang, F. C.; Zhang, J. C.; Pratt, A.; Grigorenko, A. N.; Guinea, F.; Geim, A. K.; Nair, R. R. Ultrathin Graphene-Based Membrane with Precise Molecular Sieving and Ultrafast Solvent Permeation. *Nat. Mater.* **2017**, *16* (12), 1198–1202.
- [37] Zhuravlev, L. T. The Surface Chemistry of Amorphous Silica. Zhuravlev Model. *Colloids Surfaces A Physicochem. Eng. Asp.* **2000**, *173* (1–3), 1–38.
- [38] Wang, Z.; Mao, B.; Zhao, M.; Calatayud, D. G.; Qian, W.; Li, P.; Hu, Z.; Fu, H.; Zhao, X.; Yan, S.; Kou, Z.; He, D. Ultrafast Macroscopic Assembly of High-Strength Graphene Oxide Membranes by Implanting an Interlaminar Superhydrophilic Aisle. *ACS Nano* **2022**, *16* (3), 3934-3942..
- [39] Zhang, W. H.; Yin, M. J.; Zhao, Q.; Jin, C. G.; Wang, N.; Ji, S.; Ritt, C. L.; Elimelech, M.; An, Q. F. Graphene Oxide Membranes with Stable Porous Structure for Ultrafast Water Transport. *Nat. Nanotechnol.* **2021**. *16* (3), 337-343.
- [40] Ritt, C. L.; Werber, J. R.; Deshmukh, A.; Elimelech, M. Monte Carlo Simulations of Framework Defects in Layered Two-Dimensional Nanomaterial Desalination Membranes: Implications for Permeability and Selectivity. *Environ. Sci. Technol.* **2019**, *53* (11), 6214–6224.
- [41] Liu, Y.; Zhang, F.; Zhu, W.; Su, D.; Sang, Z.; Yan, X.; Li, S.; Liang, J.; Dou, S. X. A Multifunctional Hierarchical Porous SiO₂/GO Membrane for High Efficiency Oil/Water Separation and Dye Removal. *Carbon* **2020**, *160*, 88–97.
- [42] Sun, J.; Bi, H.; Su, S.; Jia, H.; Xie, X.; Sun, L. One-Step Preparation of GO/SiO₂ Membrane for Highly Efficient Separation of Oil-in-Water Emulsion. *J. Memb.*

Sci. **2018**, *553*, 131–138.

- [43] He, Y. C.; Yang, J.; Kan, W. Q.; Zhang, H. M.; Liu, Y. Y.; Ma, J. F. A New Microporous Anionic Metal-Organic Framework as a Platform for Highly Selective Adsorption and Separation of Organic Dyes. *J. Mater. Chem. A* **2015**, *3* (4), 1675–1681.
- [44] Ranjan, P.; Verma, P.; Agrawal, S.; Rao, T. R.; Samanta, S. K.; Thakur, A. D. Inducing Dye-Selectivity in Graphene Oxide for Cationic Dye Separation Applications. *Mater. Chem. Phys.* **2019**, *226*, 350–355.
- [45] Bhattacharyya, A.; Ghorai, S.; Rana, D.; Roy, I.; Sarkar, G.; Saha, N. R.; Orasugh, J. T.; De, S.; Sadhukhan, S.; Chattopadhyay, D. Design of an Efficient and Selective Adsorbent of Cationic Dye through Activated Carbon - Graphene Oxide Nanocomposite: Study on Mechanism and Synergy. *Mater. Chem. Phys.* **2021**, *260*, 124090.
- [46] Bi, H.; Xie, X.; Yin, K.; Zhou, Y.; Wan, S.; He, L.; Xu, F.; Banhart, F.; Sun, L.; Ruoff, R. S. Spongy Graphene as a Highly Efficient and Recyclable Sorbent for Oils and Organic Solvents. *Adv. Funct. Mater.* **2012**, *22* (21), 4421–4425.
- [47] Junaidi, N. F. D.; Othman, N. H.; Fuzil, N. S.; Mat Shayuti, M. S.; Alias, N. H.; Shahrudin, M. Z.; Marpani, F.; Lau, W. J.; Ismail, A. F.; Aba, N. F. D. Recent Development of Graphene Oxide-Based Membranes for Oil–Water Separation: A Review. *Sep. Purif. Technol.* **2021**, *258*, 118000.
- [48] Scherer, M. D.; Oliveira, S. L.; Lima, S. M.; Andrade, L. H. C.; Caires, A. R. L. Determination of the Biodiesel Content in Diesel/Biodiesel Blends: A Method

Based on Fluorescence Spectroscopy. *J. Fluoresc.* **2011**, *21* (3), 1027–1031.

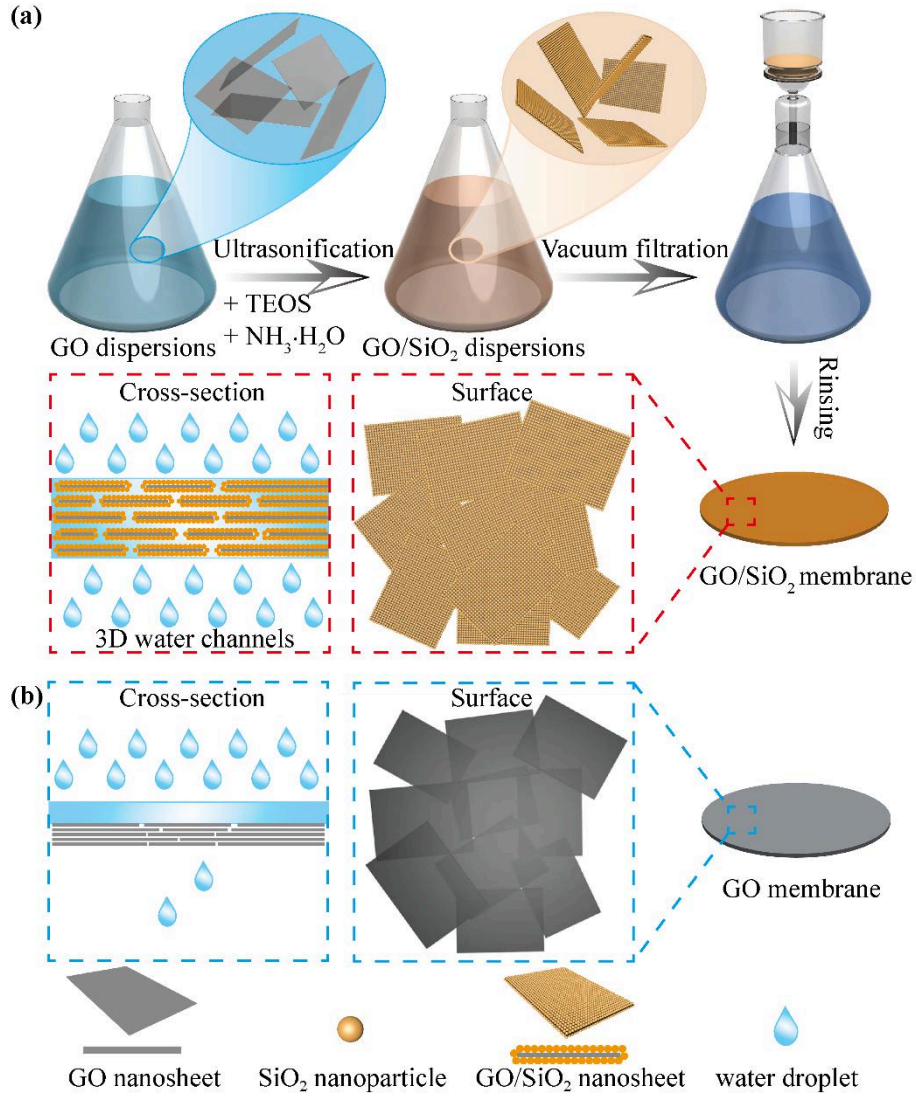


Figure 1. Design diagram of 3D water channels within GO membranes. (a) A schematic showing the constructed strategy of 3D water channels in GO/SiO₂ membranes, inserted with proposal models of surface and cross-sectional structures. (b) Schematic diagrams of surface and cross-sectional structures of GO membranes.

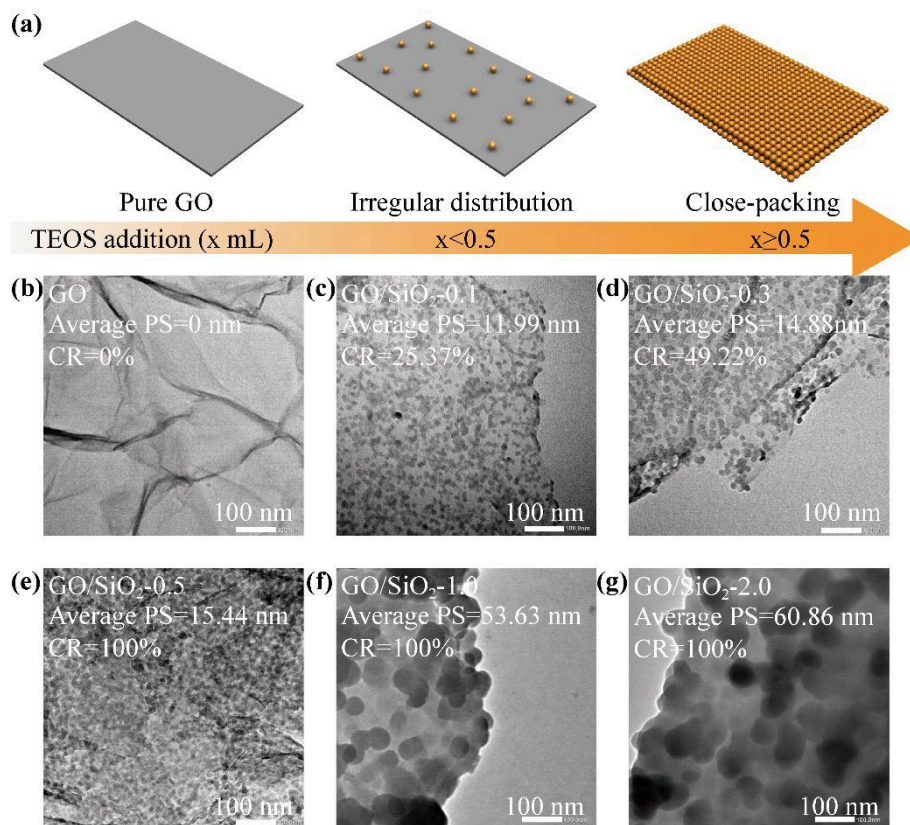


Figure 2. Growth behavior of SiO₂ nanoparticles on GO nanosheets. (a) Proposal models of *in situ* growth behavior of SiO₂ nanoparticles on GO nanosheets. (b-g) TEM images of GO/SiO₂-x dispersions (x=0, 0.1, 0.3, 0.5, 1.0 and 2.0 corresponding Fig. (b), (c), (d), (e), (f) and (g)) showing the average PS and CR of SiO₂ nanoparticles.

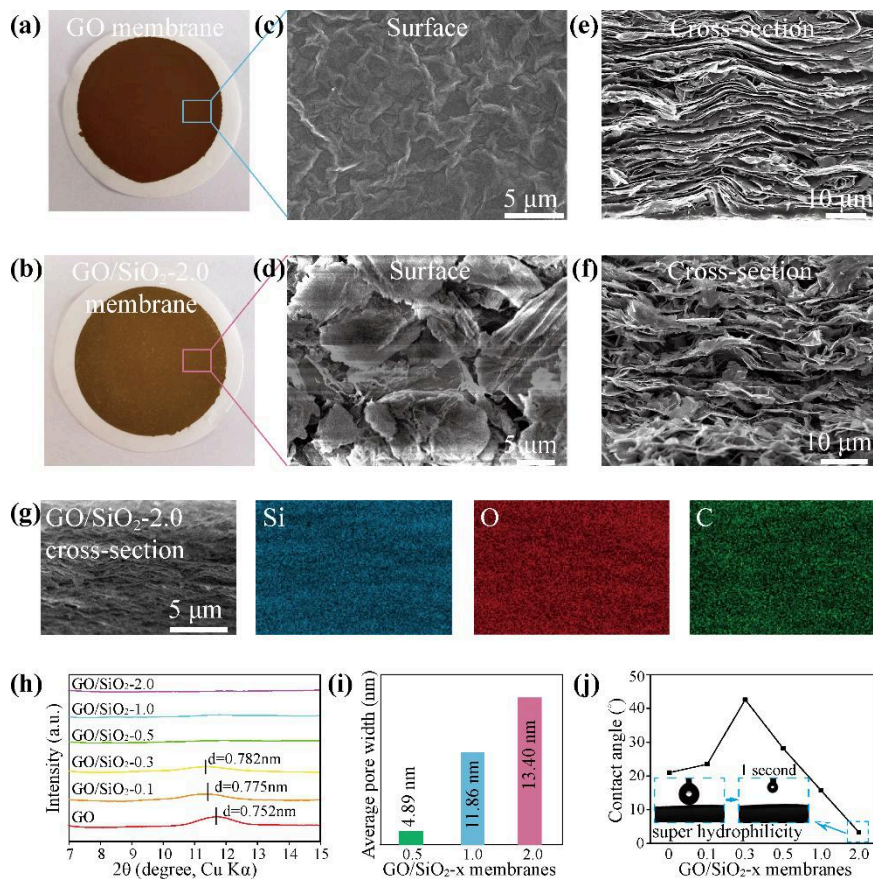


Figure 3. Structural characterizations of 3D water channels within GO membrane. (a, b) Photos of typical GO membrane (a) and GO/SiO₂-2.0 membrane (b). (c, d) Surface SEM images of typical GO membrane (c) and GO/SiO₂-2.0 membrane (d). (e, f) Cross-sectional SEM images of typical GO membrane (e) and GO/SiO₂-2.0 membrane (f). (g) Elemental mapping images of GO/SiO₂-2.0 membrane cross-section. (h) XRD patterns of GO/SiO₂-x (x=0, 0.1, 0.3, 0.5, 1.0, 2.0) membranes. (i) Average pore widths of GO/SiO₂-x membranes (x=0.5, 1.0 and 2.0) with 3D water channels. (j) Contact angles of DI water on GO/SiO₂-x (x=0, 0.1, 0.3, 0.5, 1.0 and 2.0).

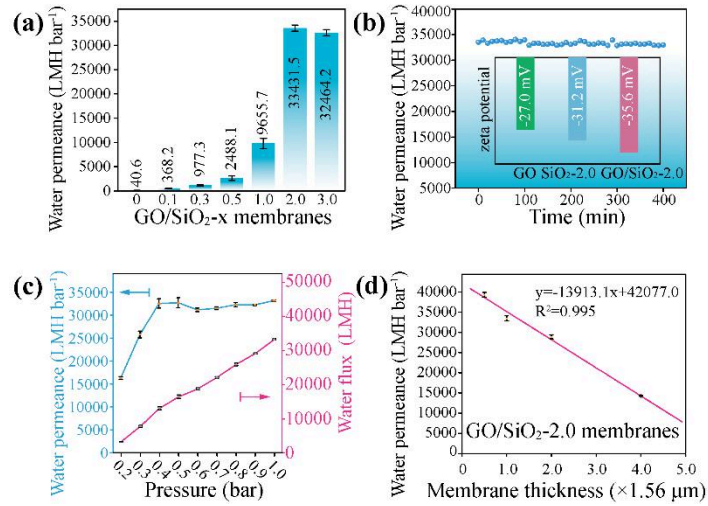


Figure 4. Water permeable performance measurements. (a) Water permeance of GO/SiO₂-x (x=0, 0.1, 0.3, 0.5, 1.0, 2.0 and 3.0) membrane under -0.08MPa. (b) Water permeance stability of the GO/SiO₂-2.0 membrane during continuous filtering operation for 400 minutes under -0.08 MPa, inserted with zeta potentials of GO dispersions, SiO₂-2.0 colloids and GO/SiO₂-2.0 dispersions. (c) Water permeance and water flux of the GO/SiO₂-2.0 membrane under different pressure. (d) Water permeance of GO/SiO₂-2.0 membranes with multiplied thicknesses under -0.08 MPa.

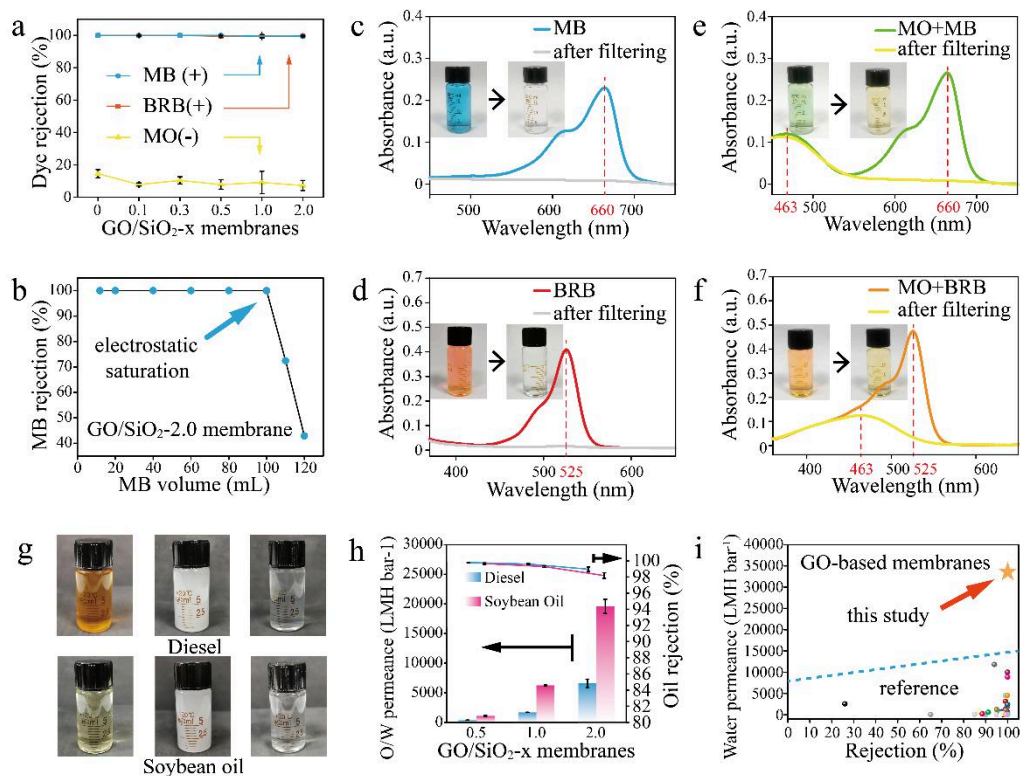


Figure 5. Purification performance measurement. (a) Dyes rejections of GO/SiO₂-x (x=0, 0.1, 0.3, 0.5, 1.0 and 2.0) membranes toward MB, BRB and MO. (b) MB Rejections of the GO/SiO₂-2.0 membrane using increasing volumes of MB solutions under -0.08 MPa. (c, d) UV spectrum and photographs of MB (c) and BRB (d) solution before and after filtering using the GO/SiO₂-2.0 membrane under -0.08 MPa. (e, f) UV spectrum and photographs of mixing dyes solution containing MO, MB (e) and MO, BRB (f) before and after filtering using GO/SiO₂-2.0 membranes under -0.08 MPa. (g) Photographs of diesel, soybean oil and their corresponding oil emulsions before and after filtering using the GO/SiO₂-2.0 membrane under -0.08 MPa. (h) O/W permeances and oil rejections of diesel and soybean oil using the GO/SiO₂-x (x=0.5, 1.0 and 2.0) membrane under -0.08 MPa. (i) Comparison of water permeance and purification performance between the GO/SiO₂-2.0 membrane and the

reported membranes in the literature (**Table S1**).

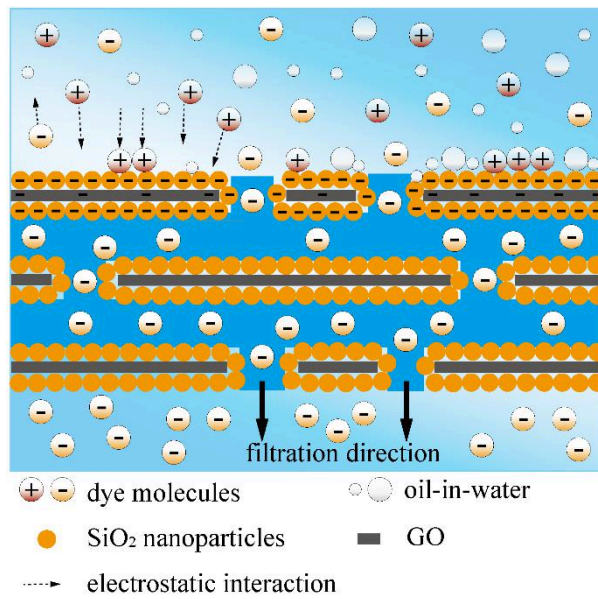


Figure 6. Mechanism diagram of well-structured 3D water channels synchronizing high water permeance and purification performance within GO membranes.

Electronic Supplementary Material

Well-structured 3D channels within GO-based membranes enable ultrafast wastewater treatment

Huaqiang Fu^{1, #}, Zhe Wang^{2, 3, #}, Peng Li² (✉), Wei Qian², Zixin Zhang¹, Xin Zhao², Hao Feng¹, Zhugen Yang⁴, Zongku Kou^{1, 3} (✉), and Daping He^{1, 2} (✉)

¹ School of Materials Science and Engineering, Wuhan University of Technology, Wuhan 430070, China

² Hubei Engineering Research Center of RF-Microwave Technology and Application, School of Science, Wuhan University of Technology, Wuhan 430070, China

³ State Key Laboratory of Advanced Technology for Materials Synthesis and Processing, Wuhan University of Technology, Wuhan 430070, China

⁴ School of Water, Energy and Environment, Cranfield University, Cranfield MK43 0AL, UK

These authors contributed equally.

Supporting information to DOI 10.1007/s12274-****-****-* (automatically inserted by the publisher)

The file includes:

Figure S1. Size distributions and coverage rates of SiO₂ nanoparticles in GO/SiO₂-x (x=0, 0.1, 0.3, 0.5, 1.0, 2.0) dispersions.

Figure S2. X-ray photoelectron spectroscopy spectrum of GO and GO/SiO₂ membranes.

Figure S3. Surface elemental mapping images of the GO membrane surface.

Figure S4. Elemental mapping images of Si on the surfaces of GO/SiO₂-x membranes.

Figure S5. Photographs of GO/SiO₂-x (x=0, 0.1, 0.3, 0.5, 1.0, 2.0) membranes prepared by using 0.5 ml GO/SiO₂-x dispersions on mixed cellulose substrates (MCE) in vacuum-assisted self-assembly method.

Figure S6. Surface SEM images of GO/SiO₂-x (x=0, 0.1, 0.3, 0.5, 1.0, 2.0) membranes.

Figure S7. Cross-sectional SEM images of GO/SiO₂-x (x=0, 0.1, 0.3, 0.5, 1.0, 2.0) corresponding to a, b, c, d, e, f) membranes prepared by using 0.5 ml GO/SiO₂-x dispersions.

Figure S8. Surface elemental mapping images of the GO/SiO₂-2.0 membrane.

Figure S9. Results of Brunauer-Emmett-Teller (BET) surface area measurements for GO/SiO₂-x (x=0.5, 1.0, 2.0) membranes.

Figure S10. Photograph and water permeance of GO/SiO₂-2.0 membranes with multiplied thicknesses.

Figure S11. Photograph of SiO₂-2.0 colloids, GO+SiO₂-2.0 dispersions and a typical GO+SiO₂-2.0 membrane.

Figure S12. TEM images and diameter distribution of SiO₂ nanoparticles in SiO₂-2.0 colloids.

Figure S13. Water permeance variance of GO+SiO₂-2.0 membranes in 10 minutes.

Figure S14. Comparison of XRD patterns between GO+SiO₂-2.0 and GO/SiO₂-2.0 membranes.

Figure S15. Schematic diagrams of water transport in the water channels of GO, GO+SiO₂-2.0 and GO/SiO₂-2.0 membranes during pressure-driven filtering process.

Figure S16. TEM image of GO+SiO₂-2.0 dispersions.

Figure S17. Ultraviolet-visible (UV) spectrum of methylene blue (MB), butyl rhodamine B (BRB) and methyl orange (MO) solutions with different concentrations and the fitting lines of concentration of dye solutions-intensity of absorption peak in UV spectrum at characteristic wavelength.

Figure S18. UV spectrum of diesel and soybean oil emulsions with different volume fractions and the fitting lines of volume fractions of oil emulsions-intensity of absorption peak in UV spectrum at characteristic wavelength.

Table S1. Comparison of water permeance and purification performance of GO-based membranes between previous studies and this work.

Other Supplementary Material for this manuscript includes the following:

Movie S1 (.avi format). Wetting process of DI water on GO/SiO₂-2.0 membranes.

Movie S2 (.avi format). Filtering process of GO/SiO₂-2.0 membranes under -0.08 MPa.

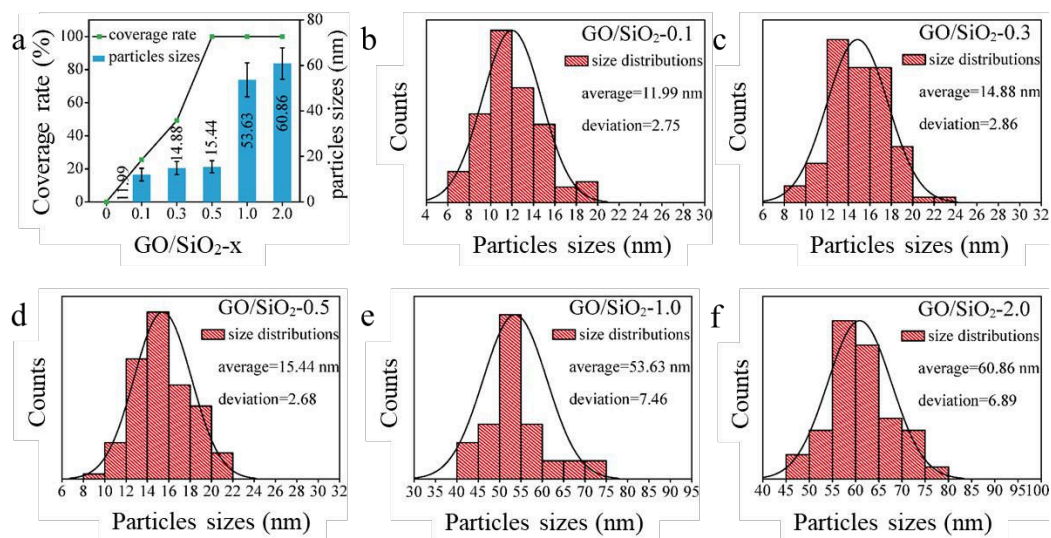


Figure S1. (a) Variation tendency of coverage rate and average particle size of SiO₂ nanoparticles on GO nanosheets. (b-f) Size distributions of SiO₂ nanoparticles in GO/SiO₂-0.1, 0.3, 0.5, 1.0 and 2.0 dispersions.

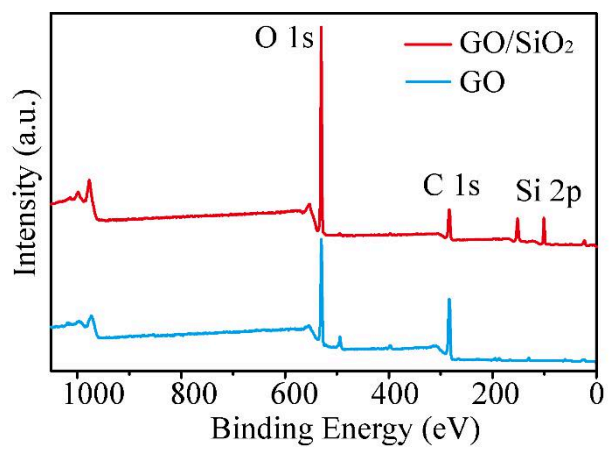


Figure S2. X-ray photoelectron spectroscopy spectrum of GO and GO/SiO₂ membranes.

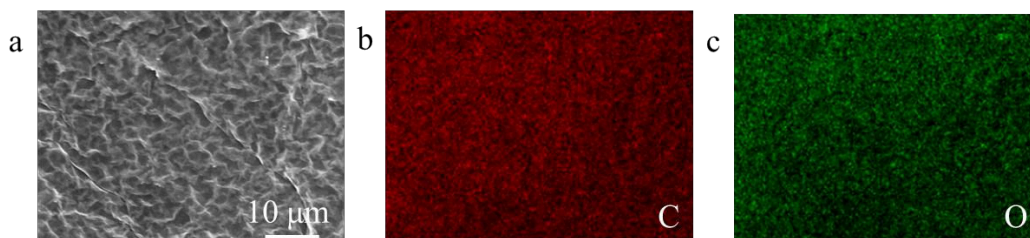


Figure S3. Surface elemental mapping images of the GO membrane surface. (a) Surface SEM image of the GO membrane. (b) Elemental mapping of carbon (C) on the GO membrane. (c) Elemental mapping of oxygen (O) on the GO membrane.

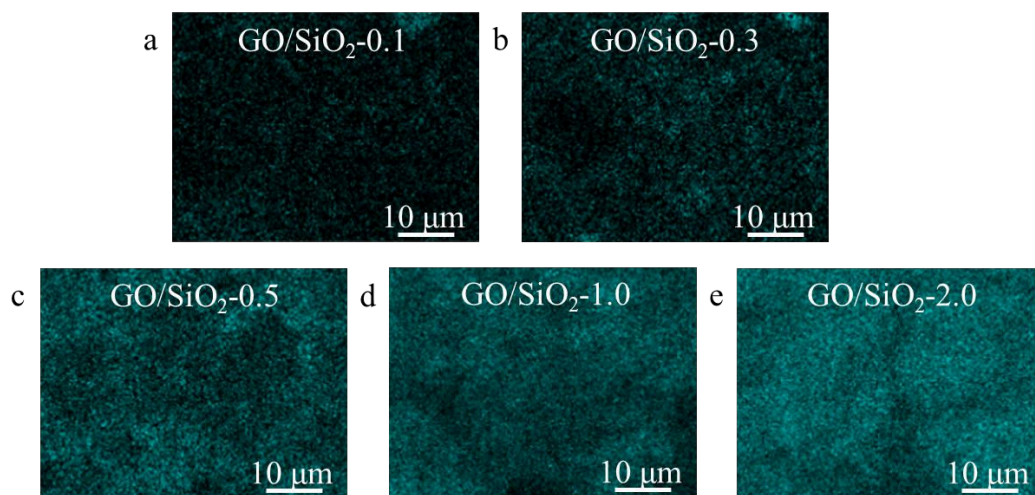


Figure S4. Elemental mapping images of Si on *the surfaces of GO/SiO₂-x membranes.*

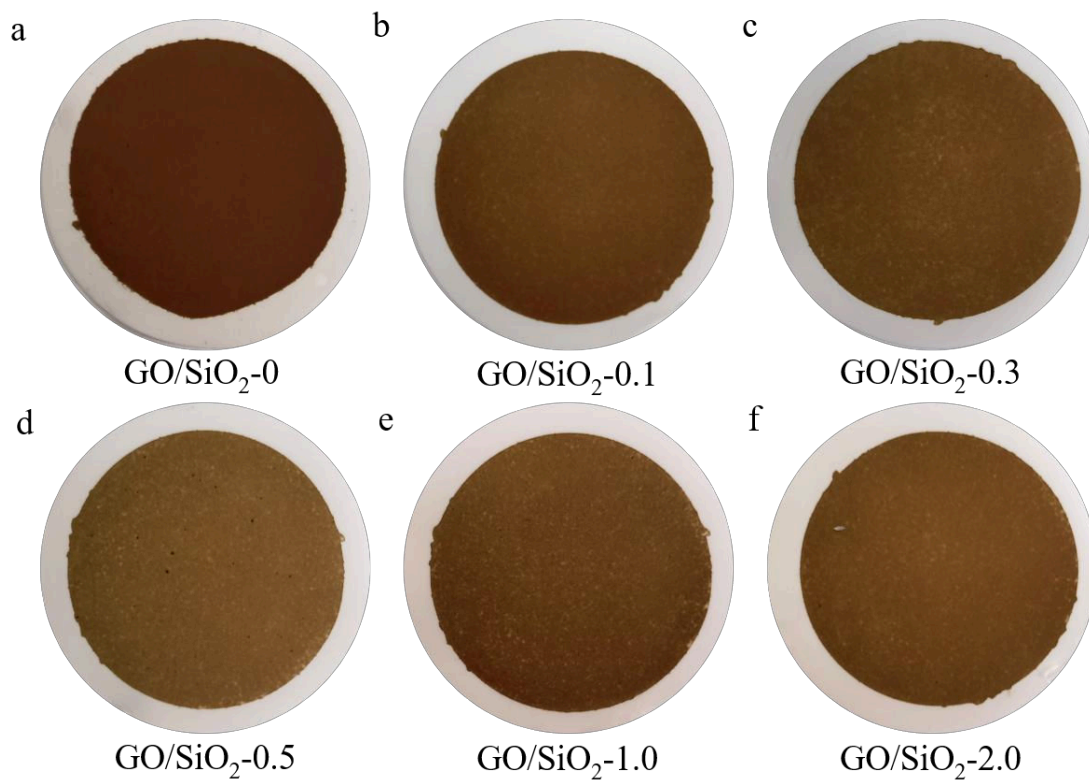


Figure S5. Photographs of GO/SiO₂-x (x=0, 0.1, 0.3, 0.5, 1.0, 2.0 corresponding to a, b, c, d, e, f) membranes prepared by using 0.5 ml GO/SiO₂-x dispersions on MCE substrates in vacuum-assisted self-assembly method.

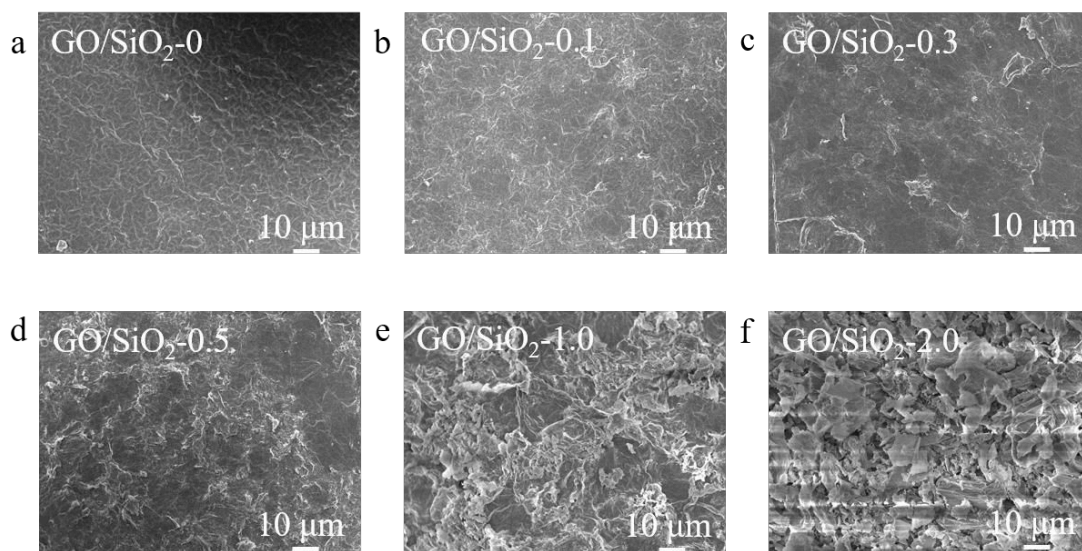


Figure S6. Surface SEM images of GO/SiO₂-x (x=0, 0.1, 0.3, 0.5, 1.0, 2.0 corresponding to a, b, c, d, e, f) membranes.

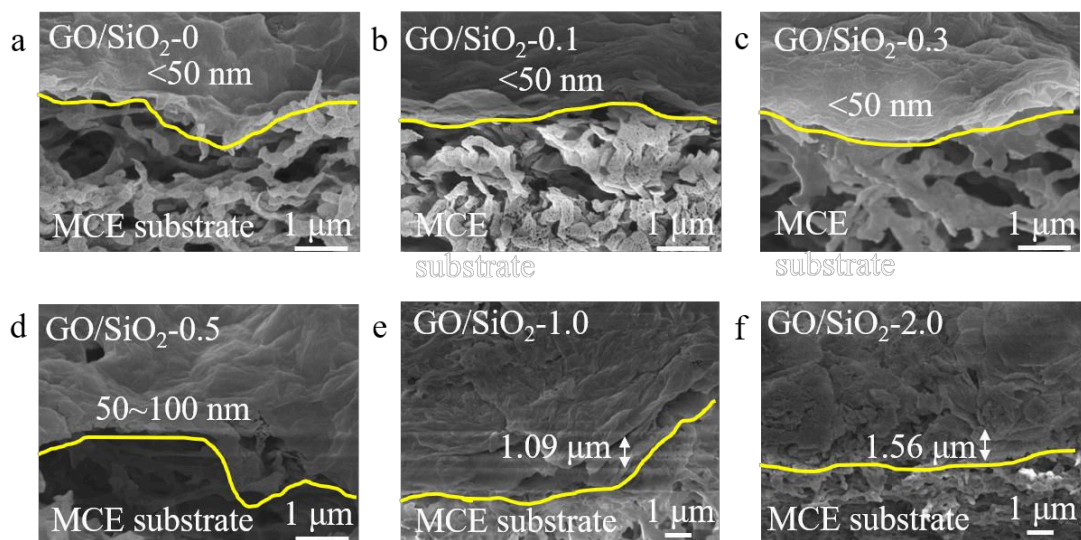


Figure S7. Cross-sectional SEM images of $\text{GO/SiO}_2\text{-}x$ ($x=0, 0.1, 0.3, 0.5, 1.0, 2.0$ corresponding to a, b, c, d, e, f) membranes prepared by using 0.5 ml $\text{GO/SiO}_2\text{-}x$ dispersions.

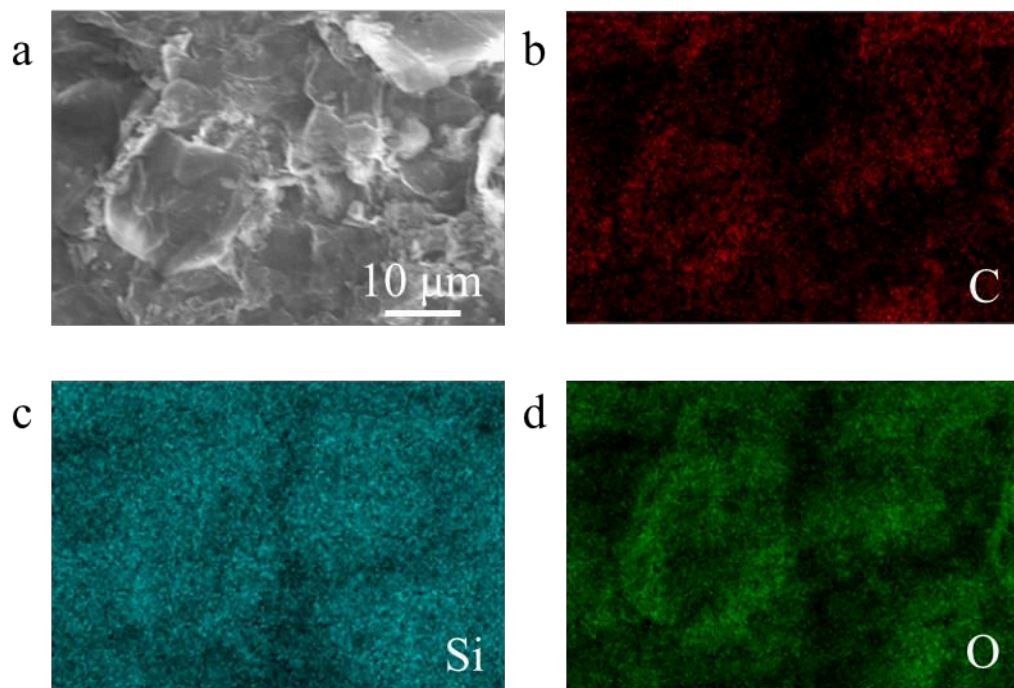


Figure S8. Surface elemental mapping images of the $GO/SiO_2-2.0$ membrane. (a) Surface SEM image of the GO membrane. (b) Elemental mapping of C on the $GO/SiO_2-2.0$ membrane. (c) Elemental mapping of Si on the $GO/SiO_2-2.0$ membrane. (d) Elemental mapping of O on the $GO/SiO_2-2.0$ membrane.

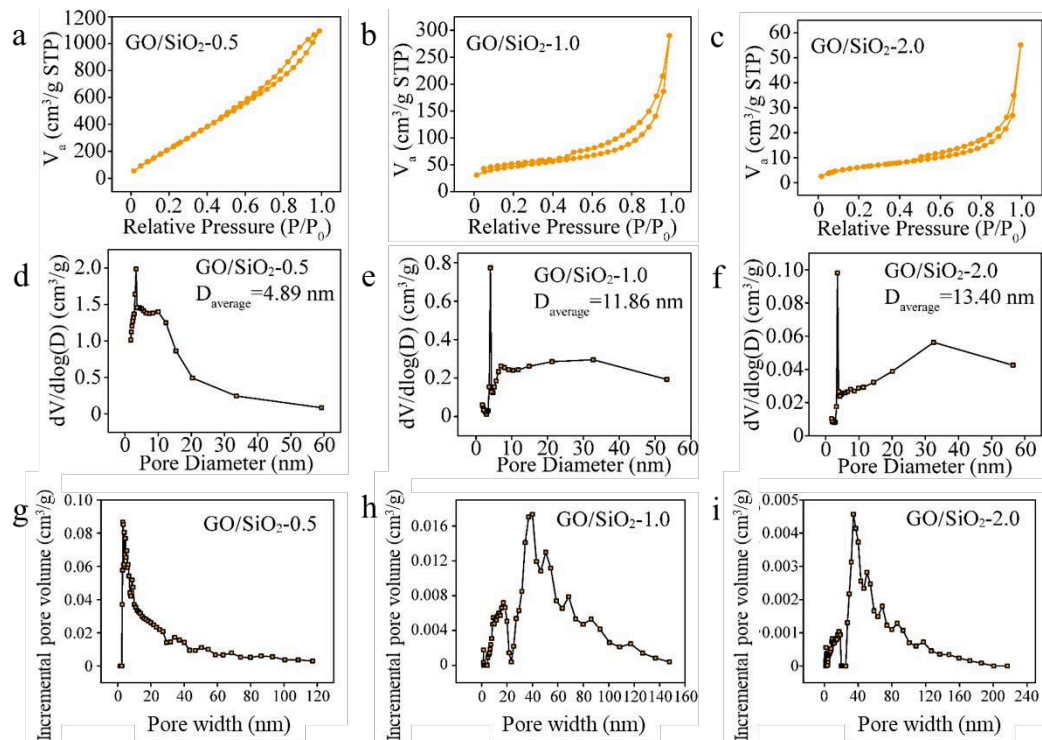


Figure S9. **Results** of Brunauer-Emmett-Teller (BET) surface area measurements for GO/SiO_2-x membranes. (a-c) N_2 adsorption-desorption isotherm of $\text{GO}/\text{SiO}_2-0.5$, 1.0 and 2.0 membranes. (d-f) Pore diameters test of $\text{GO}/\text{SiO}_2-0.5$, 1.0 and 2.0 membranes, the average pore diameters of $\text{GO}/\text{SiO}_2-0.5$, 1.0 and 2.0 membranes are 4.89 nm, 11.86 nm and 13.40 nm. (g-i) Incremental pore volume of corresponding pore width in $\text{GO}/\text{SiO}_2-0.5$, 1.0 and 2.0 membranes.

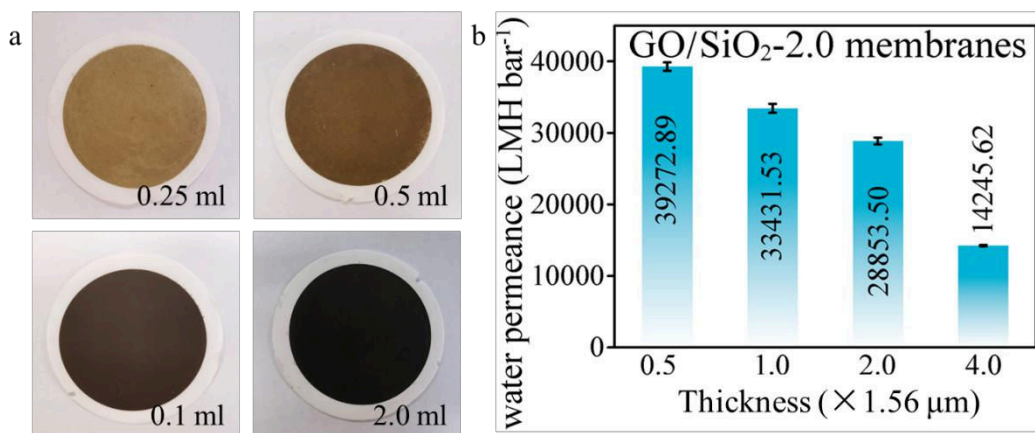


Figure S10. Photograph and water permeance of $GO/SiO_2-2.0$ membranes with multiplied thicknesses. (a) Photograph of $GO/SiO_2-2.0$ membranes prepared using different volumes (0.25 ml, 0.5 ml (master sample), 1.0 ml and 2.0 ml) of $GO/SiO_2-2.0$ dispersions. The color of membranes become deeper as the dosage of dispersions increase. (b) Water permeance of $GO/SiO_2-2.0$ membranes with multiplied thicknesses.

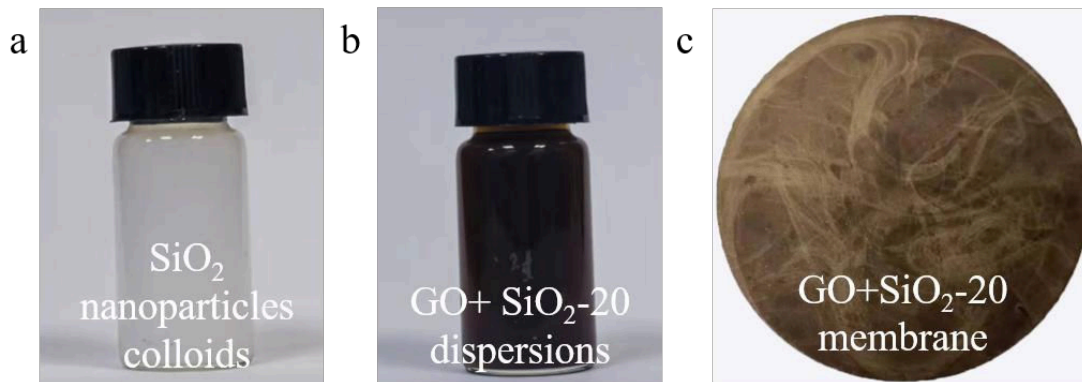


Figure S11. (a) Photograph of SiO₂-2.0 colloids. (b) Photograph of GO+SiO₂-2.0 dispersions. (c) Photograph of a typical GO+SiO₂-2.0 membrane.

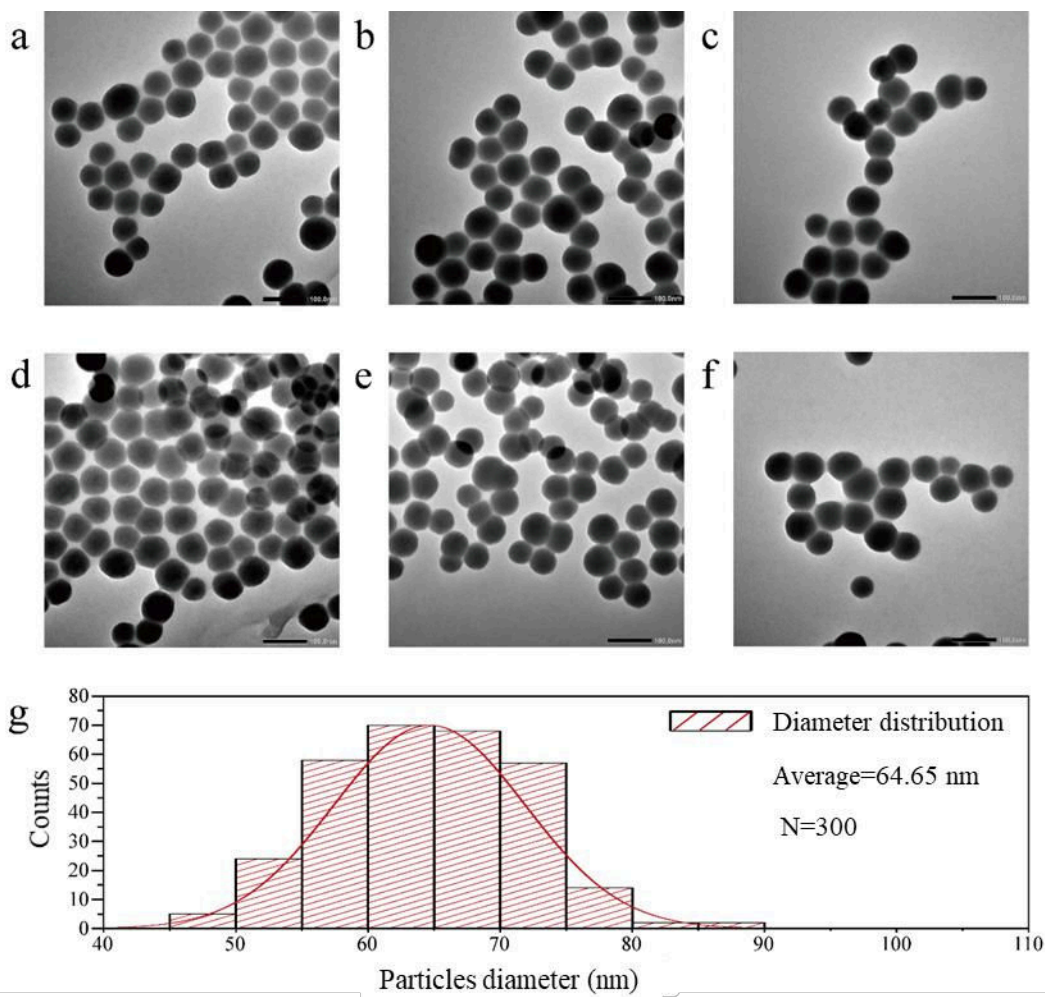


Figure S12. (a-f) TEM images of SiO₂ nanoparticles in SiO₂-2.0 colloids. (g) Diameter distribution of SiO₂ nanoparticles computed according to S12a-f.

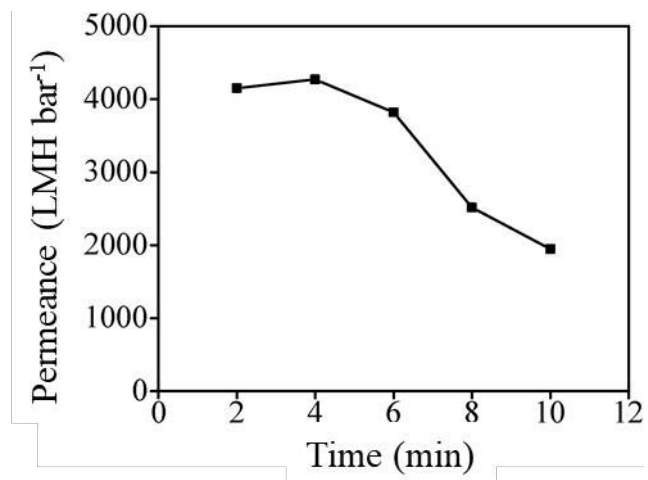


Figure S13. Water permeance variance of GO+SiO₂-2.0 membranes in 10 minutes.

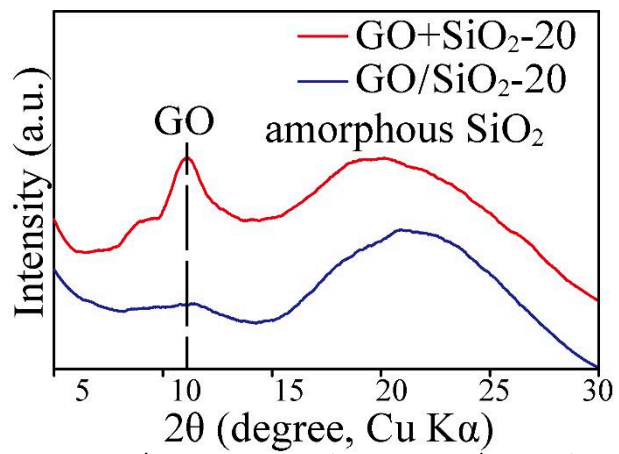


Figure S14. Comparison of XRD patterns between $GO+SiO_2-2.0$ and $GO/SiO_2-2.0$ membranes.

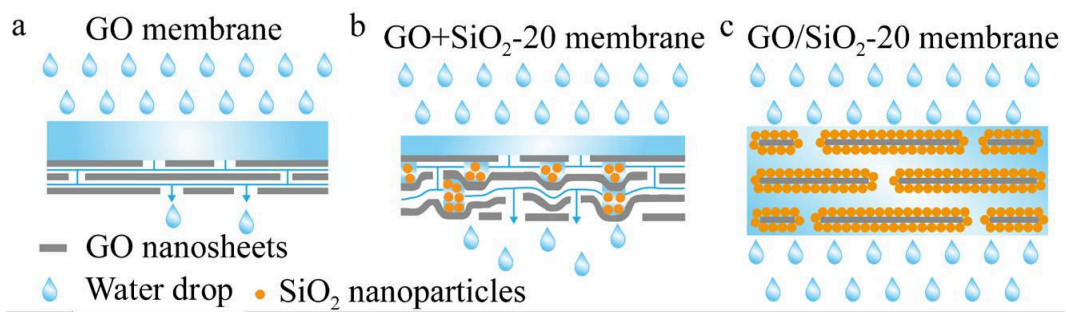


Figure S15. Schematic diagrams of water transport in the water channels of (a) GO, (b) GO+SiO₂-2.0 and (c) GO/SiO₂-2.0 membranes during pressure-driven filtering process.

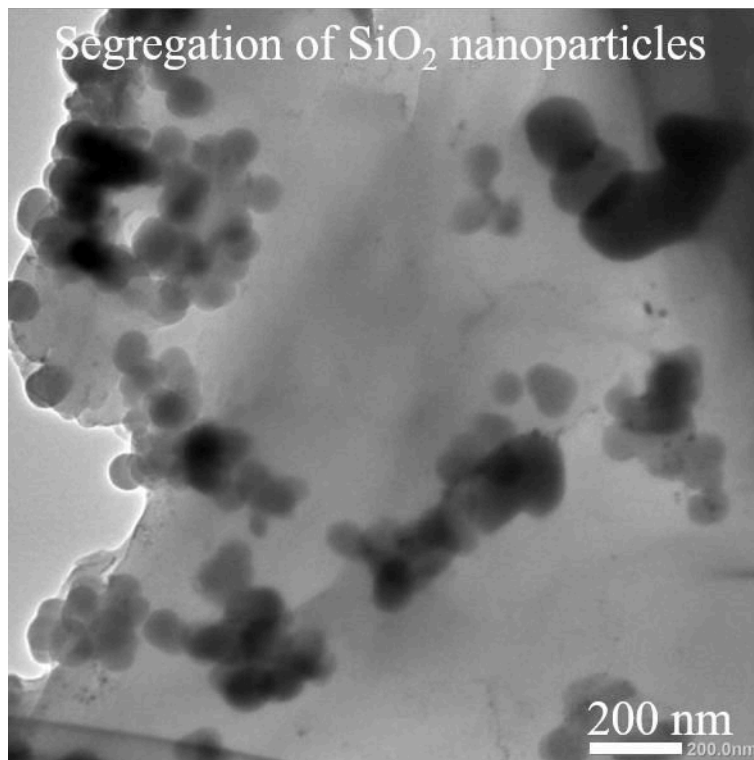


Figure S16. TEM image of GO+SiO₂-2.0 dispersions, in which the SiO₂ nanoparticles exhibit segregation.

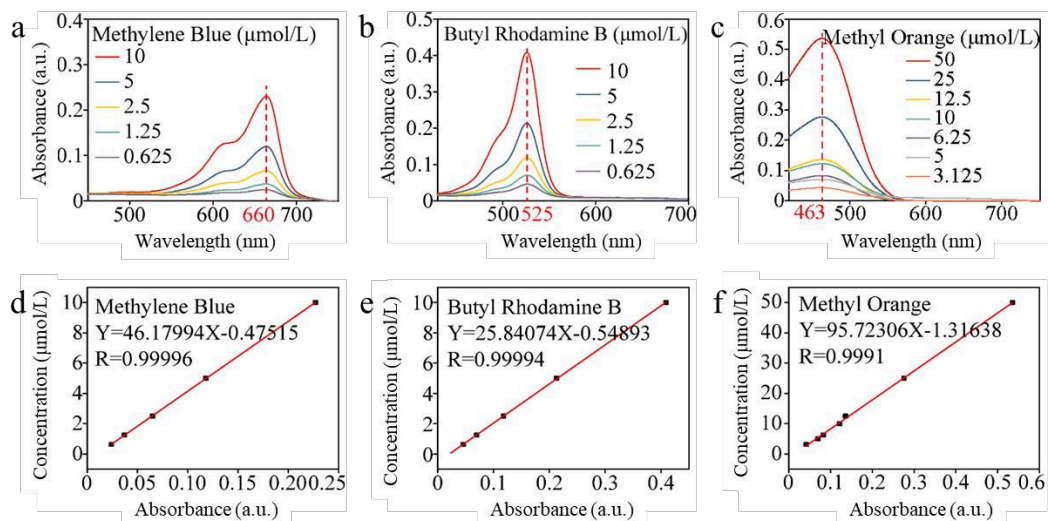


Figure S17. (a-c) UV spectrum of MB, BRB and MO solutions with different concentrations. (d-f) Fitting lines of dye solutions concentration-intensity of absorption peak in UV spectrum at characteristic wavelength. The characteristic wavelengths of MB, BRB and MO solutions are 660 nm, 525 nm and 463 nm, respectively.

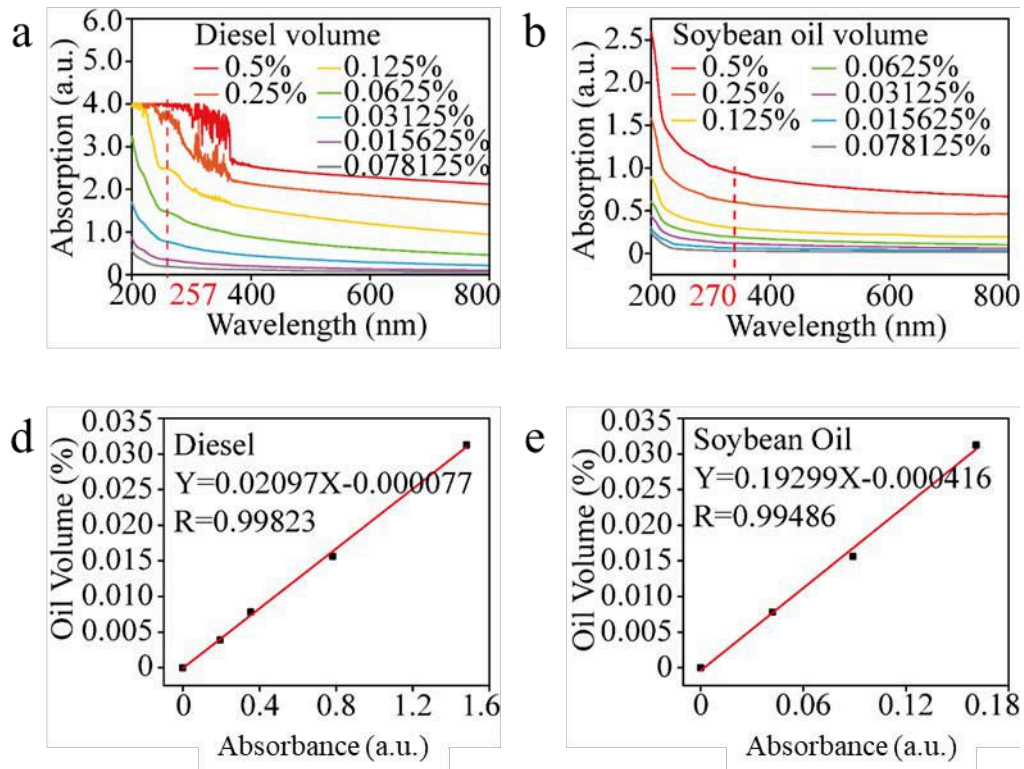


Figure S18. (a, b) UV spectrum of diesel and soybean oil emulsions with different volume fractions. (c, d) Fitting lines of oil emulsions volume fractions-intensity of absorption peak in UV spectrum at characteristic wavelength. The characteristic wavelengths of diesel and soybean oil emulsions are 257 nm and 270 nm.

Table S1. Comparison of water permeance and purification performance of GO-based membranes between previous studies and this work.

GO-based membrane	water permeance	purification performance		Ref.
	(LMH. bar ⁻¹)	oil rejection (%)	dye rejection (%)	
GO-SiO ₂ nanoparticles	4550	99	-	S1
EBl-rGO	267.1	-	100	S2
SiO ₂ /GO/EDA	2387	99.4	100	S3
PES/GO-SiO ₂	2561	26	-	S4
PAN-GO-SiO ₂	3151	99	-	S5
PDVF/RGO@SiO ₂ /PDA	528.3	80	98	S6
GO-SiO ₂	229.15	-	99	S7
SPES/GO-SiO ₂ -NH ₂	269.5	97	-	S8
GO	10	-	100	S9
GO-ZIF-8	60	-	100	S10
GO@nylon6	11.15	-	95	S11
sGO-Polyethersulfone	620	99.95	-	S12
SWCNT/GO	770	-	98.6	S13
GO/Palygorskite nanorods	1867	99.9	-	S14
D-HNTs/GO/EDA	218	99	99	S15
GO-IPDI	84.48	-	97.67	S16
rGO/PDA/g-C ₃ N ₄	23	98.3	99.8	S17
GO/g-C ₃ N ₄ @TiO ₂	4536	99.9	-	S18
HNTs@GO-PDA	1256.18	99.01	-	S19
PDA/RGO/Halloysite nanotubes	297.09	99.6	99.72	S20
GNM/SWCNT	110.6	-	96.4	S21
SFGO-La ³⁺	30	-	95	S22
GO	71	-	90	S23
NSC-GO	695	-	87	S24
GO/g-C ₃ N ₄	207	-	90	S25
GO-Mxene	71.9	-	99.5	S26
Metal-NGO/PPS	360	-	99.9	S27
UiO-rGO	30.6	-	98	S28
GO-v-COF@GO	11800	94	-	S29
EB-COF-Br	546	-	91.2	S30
SWCNT-GO	720	-	97.4	S31
GO-carbon dots	439	-	96.9	S32
g-C ₃ N ₄ -SO ₃ H-benzene moieties	8867	-	100	S33
HPEI/S-rGO	85.4	-	98.6	S34
rGO-MWCNT	1230	-	95	S35
Porous GO-HNTs	206.7	95	98.5	S36
rGO-TH	10000	-	100	S37
PVA-GO-TiO ₂	1080	99.1	-	S38
GO/g-C ₃ N ₄	30	-	100	S39
GO-SiO ₂ -EDA	2387	99.4	100	S40
GO-CNTs	11.3	-	99	S41
TICT-GO	25	-	100	S42
GO	21.8	-	99.2	S43
rGO	191	-	88.5	S44
GO-silver	139.6	-	97.1	S45
LGO	71	-	85	S46
GO	27.6	-	65	S47
GO-COF	194	-	98	S48
GO	65	-	99.9	S49
TiO ₂ -GO-PEI	26	-	99	S50
GO/SiO ₂	33431	98.2	99.6	this work

Reference

- (S1) Sun, J.; Bi, H.; Su, S.; Jia, H.; Xie, X.; Sun, L. One-Step Preparation of GO/SiO₂ Membrane for Highly Efficient Separation of Oil-in-Water Emulsion. *J. Memb. Sci.* **2018**, *553*, 131–138.
- (S2) Yi, R.; Xia, X.; Yang, R.; Yu, R.; Dai, F.; Chen, J.; Liu, W.; Wu, M.; Xu, J.; Chen, L. Selective Reduction of Epoxy Groups in Graphene Oxide Membrane for Ultrahigh Water Permeation. *Carbon* **2021**, *172*, 228–235.
- (S3) Liu, Y.; Zhang, F.; Zhu, W.; Su, D.; Sang, Z.; Yan, X.; Li, S.; Liang, J.; Dou, S. X. A Multifunctional Hierarchical Porous SiO₂/GO Membrane for High Efficiency Oil/Water Separation and Dye Removal. *Carbon* **2020**, *160*, 88–97.
- (S4) Alkindy, M. B.; Naddeo, V.; Banat, F.; Hasan, S. W. Synthesis of Polyethersulfone (PES)/GO-SiO₂ Mixed Matrix Membranes for Oily Wastewater Treatment. *Water Sci. Technol.* **2020**, *81* (7), 1354–1364.
- (S5) Naseeb, N.; Mohammed, A. A.; Laoui, T.; Khan, Z. A Novel PAN-GO-SiO₂ Hybrid Membrane for Separating Oil and Water from Emulsified Mixture. *Materials*. **2019**, *12* (2), 1–13.
- (S6) Peng, Y.; Yu, Z.; Li, F.; Chen, Q.; Yin, D.; Min, X. A Novel Reduced Graphene Oxide-Based Composite Membrane Prepared via a Facile Deposition Method for Multifunctional Applications: Oil/Water Separation and Cationic Dyes Removal. *Sep. Purif. Technol.* **2018**, *200*, 130–140.
- (S7) Du, Y. chen; Huang, L. jun; Wang, Y. xin; Yang, K.; Zhang, Z. jie; Wang, Y.; Kipper, M. J.; Belfiore, L. A.; Tang, J. guo. Preparation of Graphene Oxide/Silica Hybrid Composite Membranes and Performance Studies in Water Treatment. *J. Mater. Sci.* **2020**, *55* (25), 11188–11202.
- (S8) Kumar, M.; Sreedhar, N.; Jaoude, M. A.; Arafat, H. A. High-Flux, Antifouling Hydrophilized Ultrafiltration Membranes with Tunable Charge Density Combining Sulfonated Poly (Ether Sulfone) and Aminated Graphene Oxide Nanohybrid. *ACS Appl. Mater. Interfaces* **2020**, *12* (1), 1617–1627.
- (S9) Yang, Q.; Su, Y.; Chi, C.; Cherian, C. T.; Huang, K.; Kravets, V. G.; Wang, F. C.; Zhang, J. C.; Pratt, A.; Grigorenko, A. N.; Guinea, F.; Geim, A. K.; Nair, R. R. Ultrathin Graphene-Based Membrane with Precise Molecular Sieving and Ultrafast Solvent Permeation. *Nat. Mater.* **2017**, *16* (12), 1198–1202.
- (S10) Zhang, W. H.; Yin, M. J.; Zhao, Q.; Jin, C. G.; Wang, N.; Ji, S.; Ritt, C. L.; Elimelech, M.; An, Q. F. Graphene Oxide Membranes with Stable Porous Structure for Ultrafast Water Transport. *Nat. Nanotechnol.* **2021**, *16* (3), 337–343.
- (S11) Chen, L.; Li, Y.; Chen, L.; Li, N.; Dong, C.; Chen, Q.; Liu, B.; Ai, Q.; Si, P.; Feng, J.; Zhang, L.; Suhr, J.; Lou, J.; Ci, L. A Large-Area Free-Standing Graphene Oxide Multilayer Membrane with High Stability for Nanofiltration Applications. *Chem. Eng. J.* **2018**, *345*, 536–544.
- (S12) Qin, D.; Liu, Z.; Bai, H.; Sun, D. D.; Song, X. A New Nano-Engineered Hierarchical Membrane for Concurrent Removal of Surfactant and Oil from Oil-in-Water Nanoemulsion. *Sci. Rep.* **2016**, *6*, 1–12.
- (S13) Gao, S. J.; Qin, H.; Liu, P.; Jin, J. SWCNT-Intercalated GO Ultrathin Films for Ultrafast Separation of Molecules. *J. Mater. Chem. A* **2015**, *3* (12), 6649–6654.
- (S14) Zhao, X.; Su, Y.; Liu, Y.; Li, Y.; Jiang, Z. Free-Standing Graphene Oxide-Palygorskite Nanohybrid Membrane for Oil/Water Separation. *ACS Appl. Mater. Interfaces* **2016**, *8* (12), 8247–8256.
- (S15) Zeng, G.; He, Y.; Ye, Z.; Yang, X.; Chen, X.; Ma, J.; Li, F. Novel Halloysite Nanotubes Intercalated Graphene Oxide Based Composite Membranes for Multifunctional Applications: Oil/Water Separation and Dyes Removal. *Ind. Eng. Chem. Res.* **2017**, *56* (37), 10472–10481.
- (S16) Zhang, P.; Gong, J. L.; Zeng, G. M.; Deng, C. H.; Yang, H. C.; Liu, H. Y.; Huan, S. Y. Cross-Linking to Prepare Composite Graphene Oxide-Framework Membranes with High-Flux for Dyes and Heavy Metal Ions Removal. *Chem. Eng. J.* **2017**, *322*, 657–666.
- (S17) Li, F.; Yu, Z.; Shi, H.; Yang, Q.; Chen, Q.; Pan, Y.; Zeng, G.; Yan, L. A Mussel-Inspired Method to Fabricate Reduced Graphene Oxide/g-C₃N₄ Composites Membranes for Catalytic Decomposition and Oil-in-Water Emulsion Separation. *Chem. Eng. J.* **2017**, *322*, 33–45.
- (S18) Liu, Y.; Su, Y.; Guan, J.; Cao, J.; Zhang, R.; He, M.; Gao, K.; Zhou, L.; Jiang, Z. 2D Heterostructure Membranes with Sunlight-Driven Self-Cleaning Ability for Highly Efficient Oil-Water Separation. *Adv. Funct. Mater.* **2018**, *28* (13), 1–10.
- (S19) Zhan, Y.; He, S.; Wan, X.; Zhao, S.; Bai, Y. Thermally and Chemically Stable Poly(Arylene Ether Nitrile)/Halloysite Nanotubes Intercalated Graphene Oxide Nanofibrous Composite Membranes for Highly Efficient Oil/Water Emulsion Separation in Harsh Environment. *J. Memb. Sci.* **2018**, *567*, 76–88.
- (S20) Liu, Y.; Tu, W.; Chen, M.; Ma, L.; Yang, B.; Liang, Q.; Chen, Y. A Mussel-Induced Method to Fabricate Reduced Graphene Oxide/Halloysite Nanotubes Membranes for Multifunctional Applications in Water Purification and Oil/Water Separation. *Chem. Eng. J.* **2018**, *336*, 263–277.
- (S21) Yang, Y.; Yang, X.; Liang, L.; Gao, Y.; Cheng, H.; Li, X.; Zou, M.; Ma, R.; Yuan, Q.; Duan, X. Large-Area Graphene-Nanomesh/Carbon-Nanotube Hybrid Membranes for Ionic and Molecular Nanofiltration. *Science* **2019**, *364* (6445), 1057–1062.
- (S22) Nie, L.; Goh, K.; Wang, Y.; Lee, J.; Huang, Y.; Karahan, H. E.; Zhou, K.; Quiver, M. D.; Bae, T.-H. Realizing Small-Flake Graphene Oxide Membranes for Ultrafast Size-Dependent Organic Solvent Nanofiltration. *Sci. Adv.* **2020**, *6* (17), eaaz9184.
- (S23) Akbari, A.; Sheath, P.; Martin, S. T.; Shinde, D. B.; Shaibani, M.; Banerjee, P. C.; Tkacz, R.; Bhattacharyya, D.; Majumder, M. Large-Area Graphene-Based Nanofiltration Membranes by Shear Alignment of Discotic Nematic Liquid Crystals of Graphene Oxide. *Nat. Commun.* **2016**, *7* (1), 1–12.
- (S24) Huang, H.; Song, Z.; Wei, N.; Shi, L.; Mao, Y.; Ying, Y.; Sun, L.; Xu, Z.; Peng, X. Ultrafast Viscous Water

- Flow through Nanostrand-Channelled Graphene Oxide Membranes. *Nat. Commun.* **2013**, *4* (1), 1–9.
- (S25) Wu, Z.; Gao, L.; Wang, J.; Zhao, F.; Fan, L.; Hua, D.; Japip, S.; Xiao, J.; Zhang, X.; Zhou, S. F.; Zhan, G. Preparation of Glycine Mediated Graphene Oxide/g-C₃N₄ Lamellar Membranes for Nanofiltration. *J. Memb. Sci.* **2020**, *601*, 117948.
- (S26) Liu, T.; Liu, X.; Graham, N.; Yu, W.; Sun, K. Two-Dimensional MXene Incorporated Graphene Oxide Composite Membrane with Enhanced Water Purification Performance. *J. Memb. Sci.* **2020**, *593*, 117431.
- (S27) Gao, Y.; Su, K.; Wang, X.; Li, Z. A Metal-Nano GO Frameworks/PPS Membrane with Super Water Flux and High Dyes Interception. *J. Memb. Sci.* **2019**, *574*, 55–64.
- (S28) Guan, K.; Zhao, D.; Zhang, M.; Shen, J.; Zhou, G.; Liu, G.; Jin, W. 3D Nanoporous Crystals Enabled 2D Channels in Graphene Membrane with Enhanced Water Purification Performance. *J. Memb. Sci.* **2017**, *542*, 41–51.
- (S29) Liu, Y.; Guan, J.; Su, Y.; Zhang, R.; Cao, J.; He, M.; Yuan, J.; Wang, F.; You, X.; Jiang, Z. Graphene Oxide Membranes with an Ultra-Large Interlayer Distance through Vertically Grown Covalent Organic Framework Nanosheets. *J. Mater. Chem. A* **2019**, *7* (44), 25458–25466.
- (S30) Zhang, W.; Zhang, L.; Zhao, H.; Li, B.; Ma, H. A Two-Dimensional Cationic Covalent Organic Framework Membrane for Selective Molecular Sieving. *J. Mater. Chem. A* **2018**, *6* (27), 13331–13339.
- (S31) Gao, S. J.; Qin, H.; Liu, P.; Jin, J. SWCNT-Intercalated GO Ultrathin Films for Ultrafast Separation of Molecules. *J. Mater. Chem. A* **2015**, *3* (12), 6649–6654.
- (S32) Wang, W.; Eftekhari, E.; Zhu, G.; Zhang, X.; Yan, Z.; Li, Q. Graphene Oxide Membranes with Tunable Permeability Due to Embedded Carbon Dots. *Chem. Commun.* **2014**, *50* (86), 13089–13092.
- (S33) Ran, J.; Pan, T.; Wu, Y.; Chu, C.; Cui, P.; Zhang, P.; Ai, X.; Fu, C.; Yang, Z.; Xu, T. Endowing G-C₃N₄ Membranes with Superior Permeability and Stability by Using Acid Spacers. *Angew. Chemie* **2019**, *131* (46), 16615–16620.
- (S34) Huang, L.; Chen, J.; Gao, T.; Zhang, M.; Li, Y.; Dai, L.; Qu, L.; Shi, G. Reduced Graphene Oxide Membranes for Ultrafast Organic Solvent Nanofiltration. *Adv. Mater.* **2016**, *28* (39), 8669–8674.
- (S35) Goh, K.; Jiang, W.; Karahan, H. E.; Zhai, S.; Wei, L.; Yu, D.; Fane, A. G.; Wang, R.; Chen, Y. All-Carbon Nanoarchitectures as High-Performance Separation Membranes with Superior Stability. *Adv. Funct. Mater.* **2015**, *25* (47), 7348–7359.
- (S36) Guan, J.; You, X.; Shi, B.; Liu, Y.; Yuan, J.; Yang, C.; Pang, X.; Wu, H.; Shen, J.; Fan, C.; Long, M.; Zhang, R.; Jiang, Z. Engineering Multi-Pathway Graphene Oxide Membranes toward Ultrafast Water Purification. *J. Memb. Sci.* **2021**, *638*, 119706.
- (S37) Thebo, K. H.; Qian, X.; Zhang, Q.; Chen, L.; Cheng, H. M.; Ren, W. Highly Stable Graphene-Oxide-Based Membranes with Superior Permeability. *Nat. Commun.* **2018**, *9* (1), 1–8.
- (S38) Zhong, Q.; Shi, G.; Sun, Q.; Mu, P.; Li, J. Robust PVA-GO-TiO₂ Composite Membrane for Efficient Separation Oil-in-Water Emulsions with Stable High Flux. *J. Memb. Sci.* **2021**, *640*, 119836.
- (S39) Wu, Y.; Fu, C. F.; Huang, Q.; Zhang, P.; Cui, P.; Ran, J.; Yang, J.; Xu, T. 2D Heterostructured Nanofluidic Channels for Enhanced Desalination Performance of Graphene Oxide Membranes. *ACS Nano* **2021**, *15* (4), 7586–7595.
- (S40) Liu, Y.; Zhang, F.; Zhu, W.; Su, D.; Sang, Z.; Yan, X.; Li, S.; Liang, J.; Dou, S. X. A Multifunctional Hierarchical Porous SiO₂/GO Membrane for High Efficiency Oil/Water Separation and Dye Removal. *Carbon* **2020**, *160*, 88–97.
- (S41) Han, Y.; Jiang, Y.; Gao, C. High-Flux Graphene Oxide Nanofiltration Membrane Intercalated by Carbon Nanotubes. *ACS Appl. Mater. Interfaces* **2015**, *7* (15), 8147–8155.
- (S42) Kang, K. M.; Kim, D. W.; Ren, C. E.; Cho, K. M.; Kim, S. J.; Choi, J. H.; Nam, Y. T.; Gogotsi, Y.; Jung, H. T. Selective Molecular Separation on Ti₃C₂T_x-Graphene Oxide Membranes during Pressure-Driven Filtration: Comparison with Graphene Oxide and MXenes. *ACS Appl. Mater. Interfaces* **2017**, *9* (51), 44687–44694.
- (S43) Han, Y.; Xu, Z.; Gao, C. Ultrathin Graphene Nanofiltration Membrane for Water Purification. *Adv. Funct. Mater.* **2013**, *23* (29), 3693–3700.
- (S44) Ying, Y.; Sun, L.; Wang, Q.; Fan, Z.; Peng, X. In-Plane Mesoporous Graphene Oxide Nanosheet Assembled Membranes for Molecular Separation. *RSC Adv.* **2014**, *4* (41), 21425–21428.
- (S45) Liu, G. F.; Huang, L. J.; Wang, Y. X.; Tang, J. G.; Wang, Y.; Cheng, M. M.; Zhang, Y.; Kipper, M. J.; Belfiore, L. A.; Ranil, W. S. Preparation of a Graphene/Silver Hybrid Membrane as a New Nanofiltration Membrane. *RSC Adv.* **2017**, *7* (77), 49159–49165.
- (S46) Huang, H.; Mao, Y.; Ying, Y.; Liu, Y.; Sun, L.; Peng, X. Salt Concentration, PH and Pressure Controlled Separation of Small Molecules through Lamellar Graphene Oxide Membranes. *Chem. Commun.* **2013**, *49* (53), 5963–5965.
- (S47) Hu, M.; Mi, B. Enabling Graphene Oxide Nanosheets as Water Separation Membranes. *Environ. Sci. Technol.* **2013**, *47* (8), 3715–3723.
- (S48) Sui, X.; Yuan, Z.; Liu, C.; Wei, L.; Xu, M.; Liu, F.; Montoya, A.; Goh, K.; Chen, Y. Graphene Oxide Laminates Intercalated with 2D Covalent-Organic Frameworks as a Robust Nanofiltration Membrane. *J. Mater. Chem. A* **2020**, *8* (19), 9713–9725.
- (S49) Shen, Y. X.; Song, W. C.; Ryan Barden, D.; Ren, T.; Lang, C.; Feroz, H.; Henderson, C. B.; Saboe, P. O.; Tsai, D.; Yan, H.; Butler, P. J.; Bazan, G. C.; Phillip, W. A.; Hickey, R. J.; Cremer, P. S.; Vashisth, H.; Kumar, M. Achieving High Permeability and Enhanced Selectivity for Angstrom-Scale Separations Using Artificial

Water Channel Membranes. *Nat. Commun.* **2018**, *9* (1), 1–11.
(S50) Zheng, K.; Li, S.; Chen, Z.; Chen, Y.; Hong, Y.; Lan, W. Highly Stable Graphene Oxide Composite Nanofiltration Membrane. *Nanoscale* **2021**, *13* (22), 10061–10066.